Searching for quantum-gravity footprint around stellar-mass black holes

Luigi Foschini[1], Alberto Vecchiato[2], Alfio Maurizio Bonanno[3]

(1) Osservatorio Astronomico di Brera — Istituto Nazionale di Astrofisica (INAF), Merate, Italy
(2) Osservatorio Astrofisico di Torino — Istituto Nazionale di Astrofisica (INAF), Pino Torinese, Italy
(3) Osservatorio Astrofisico di Catania — Istituto Nazionale di Astrofisica (INAF), Catania, Italy

4th International FLAG Workshop: The Quantum and Gravity
9th-11th September 2024 – Villa Cerami, Catania

Background image credit: International Centre for Radio Astronomy Research.

Asymptotically Safe Gravity (Weinberg 1979; see Bonanno et al. 2020 for a review)

Reuter & Weyer (2004): observational footprints on astrophysical scales (cosmological, galactic)?

$$G(r) \sim G_{\rm N}\left(1 - \frac{\xi}{r^2}\right) \qquad r \gg l_{\rm Planck} \qquad 0 < \xi < 1$$

Observational footprints around Kerr black holes?
(Reuter & Tuiran 2010; Haroon et al. 2018; Eichhorn & Held 2022; Sánchez 2024)

Co-rotating ($a^\star = 0.98$, $\tilde{\xi}_{c+} = 0.0199$)		Counter-rotating ($a^\star = 0.98$, $\tilde{\xi}_{c+} = 0.0199$)	
$\tilde{\xi}$	$x_{\rm isco}$	$\tilde{\xi}$	$x_{\rm isco}$
0	1.6140	0	8.9437
0.010	1.4715	0.010	8.9373
0.019	1.2075	0.019	8.9315

Table I. The value of $x_{\rm isco}$ for $a^\star = 0.98$ and for different values of $\tilde{\xi}$. The left column is for prograde motion while the right column is for retrograde motion.

Co-rotating ($a^\star = 0.3$, $\tilde{\xi}_{c+} = 0.5331$)		Counter-rotating ($a^\star = 0.3$, $\tilde{\xi}_{c+} = 0.5331$)	
$\tilde{\xi}$	$x_{\rm isco}$	$\tilde{\xi}$	$x_{\rm isco}$
0	4.9786	0	6.9493
0.40	4.3171	0.25	6.7205
0.50	4.0861	0.50	6.4659

Table II. The value of $x_{\rm isco}$ for $a^\star = 0.3$ and for different values of $\tilde{\xi}$. The left column is for prograde motion while the right column is for retrograde motion.

One possible effect of ASG:
- more compact BH, event horizon, photosphere
- smaller innermost stable circular orbit (isco) than that expected from general relativity (**Sánchez 2024**)

"irrespective of theoretical considerations, any observational avenue to put constrains on deviations from GR, should be explored." [A. Eichhorn & A. Held, 2023]

The radius of the innermost stable circular orbit (isco) around a rotating black hole

What do we need to know?

The radius of the innermost stable circular orbit (isco) around a rotating black hole

What do we need to know?

To calculate the theoretical r_{isco}:

- Mass of the black hole (→ gravitational radius);
- Spin (*a*);

The radius of the innermost stable circular orbit (isco) around a rotating black hole

What do we need to know?

To calculate the theoretical r_{isco}:

- Mass of the black hole (→ gravitational radius);
- Spin (*a*);

$$r_{\rm isco} = r_{\rm g}\left[3 + Z_2 - \sqrt{(3 - Z_2)(3 + Z_1 + 2Z_2)}\right]$$

$$Z_1 = 1 + \sqrt[3]{1 - a^2}\left[\sqrt[3]{1 + a} + \sqrt[3]{1 - a}\right]$$

$$Z_2 = \sqrt{3a^2 + Z_1^2}$$

The radius of the innermost stable circular orbit (isco) around a rotating black hole

What do we need to know?

To calculate the theoretical r_{isco}:

- Mass of the black hole (→ gravitational radius);
- Spin (*a*);

$$r_{\rm isco} = r_{\rm g}\left[3 + Z_2 - \sqrt{(3 - Z_2)(3 + Z_1 + 2Z_2)}\right]$$

$$Z_1 = 1 + \sqrt[3]{1 - a^2}\left[\sqrt[3]{1 + a} + \sqrt[3]{1 - a}\right]$$

$$Z_2 = \sqrt{3a^2 + Z_1^2}$$

To measure the observed r_{isco}:

- Spectrum of the accretion disk (→ temperature of the inner disk);
- Inclination of the accretion disk (*i*, viewing angle);
- Distance from the Earth (*d*);

The radius of the innermost stable circular orbit (isco) around a rotating black hole

What do we need to know?

To calculate the theoretical r_{isco}:

- Mass of the black hole (→ gravitational radius);
- Spin (a);

$$r_{\rm isco} = r_{\rm g}\left[3 + Z_2 - \sqrt{(3-Z_2)(3+Z_1+2Z_2)}\right]$$

$$Z_1 = 1 + \sqrt[3]{1-a^2}\left[\sqrt[3]{1+a} + \sqrt[3]{1-a}\right]$$

$$Z_2 = \sqrt{3a^2 + Z_1^2}$$

To measure the observed r_{isco}:

- Spectrum of the accretion disk (→ temperature of the inner disk);
- Inclination of the accretion disk (i, viewing angle);
- Distance from the Earth (d);

Best candidates: **stellar-mass black holes**

- the smaller, the better, because the ASG effects should be greater;
- accretion disk spectrum peaks in the soft X-rays (less problems than supermassive BH, peaking in UV);
- high statistics.

Spectrum of the accretion disk: multicolour black body (Mitsuda et al. 1984)

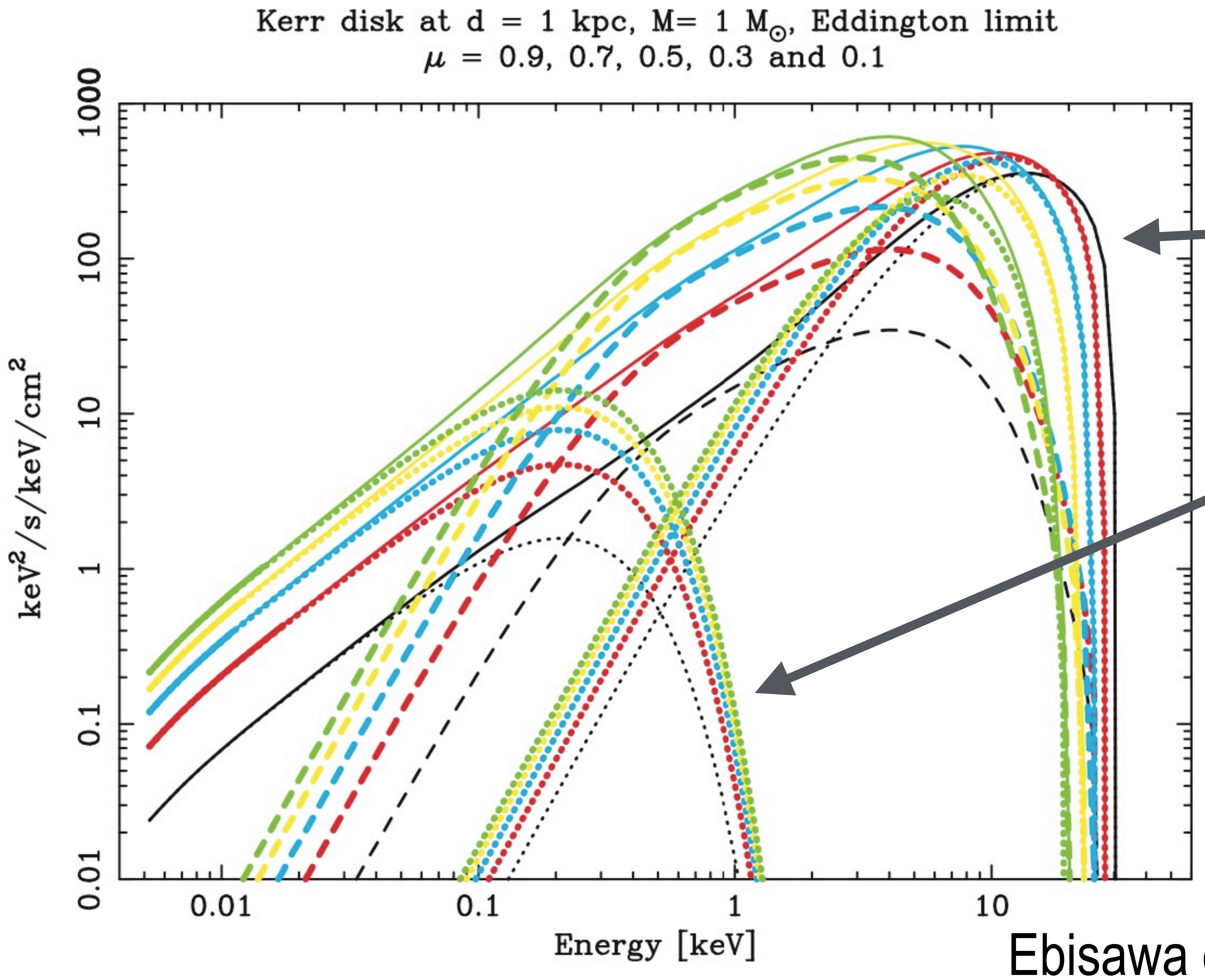

Ebisawa et al. (2003)

Fig. 2.—Kerr accretion disk spectra with an extreme angular momentum ($a = 0.998$), observed at the inclination angle $\mu \equiv \cos i = 0.9$ (*green*; near face-on), 0.7 (*yellow*), 0.5 (*cyan*), 0.3 (*red*), and 0.1 (*black*; near edge-on). Note the units of the ordinate (keV^2 s^{-1} keV^{-1} cm^{-2}), which facilitate seeing the energy release per logarithmic energy. Solid lines indicate the total disk spectra, and contributions from inner ($1.26r_g < r < 7r_g$), middle ($7r_g < r < 400r_g$), and outer parts ($400r_g < r$) are plotted separately with either dotted or broken lines. The distance and mass are assumed to be 1 kpc and 1 $M_\odot$, respectively. The Eddington luminosity is assumed, and $T_{\rm col}/T_{\rm eff} = 1$.

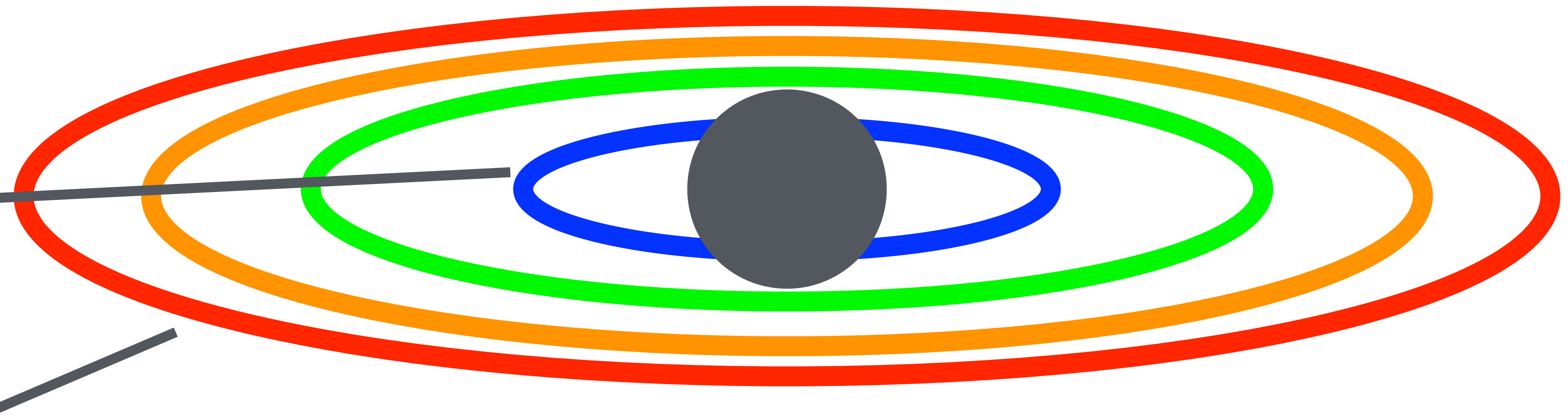

The accretion disk is divided into rings, each one a black body with increasing peak temperature with decreasing distance from the black hole.

Peak temperature → matter closest to the BH, *but*…

Spectrum of the accretion disk: multicolour black body (Mitsuda et al. 1984)

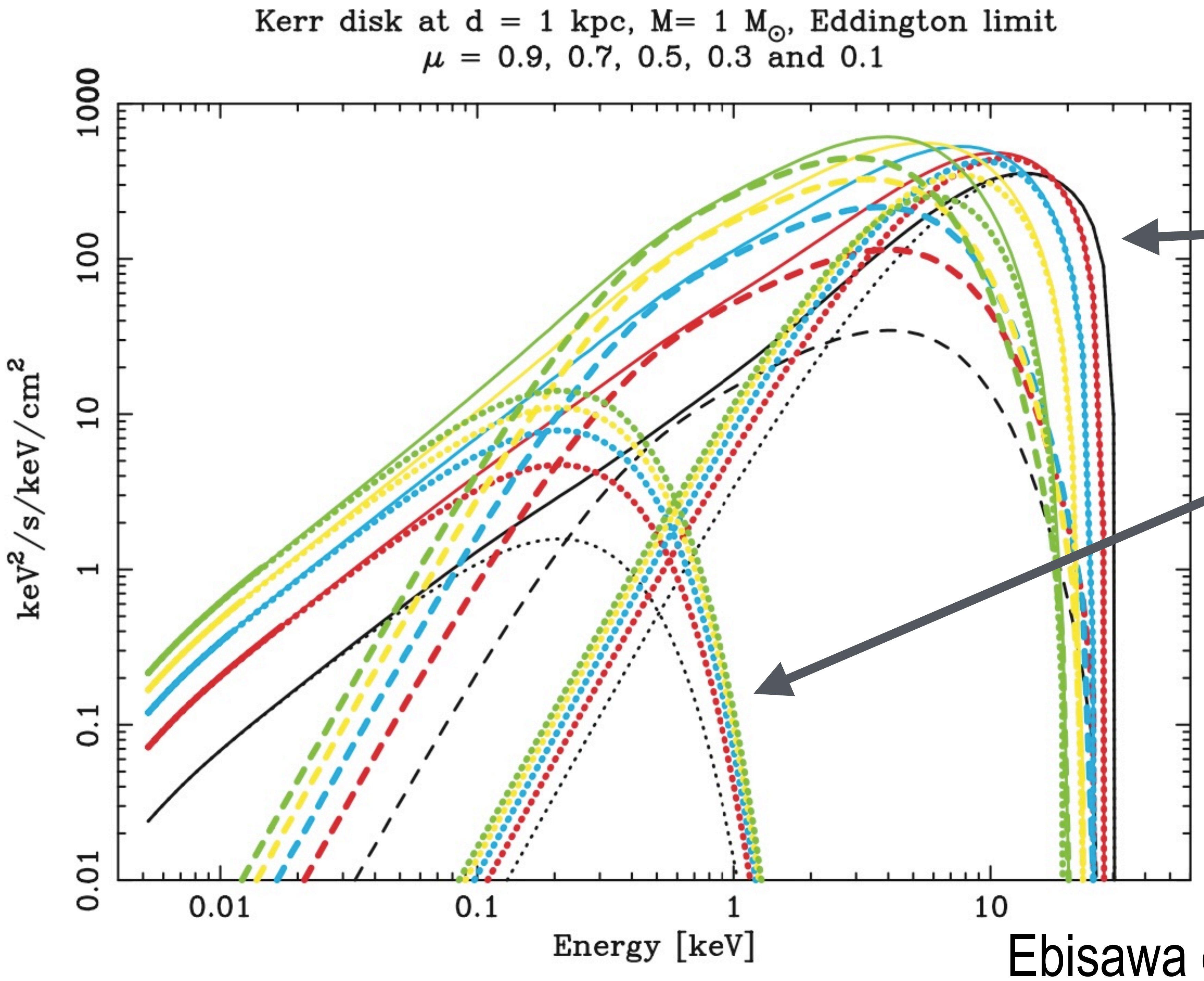

Ebisawa et al. (2003)

FIG. 2.—Kerr accretion disk spectra with an extreme angular momentum ($a = 0.998$), observed at the inclination angle $\mu \equiv \cos i = 0.9$ (*green*; near face-on), 0.7 (*yellow*), 0.5 (*cyan*), 0.3 (*red*), and 0.1 (*black*; near edge-on). Note the units of the ordinate (keV^2 s^{-1} keV^{-1} cm^{-2}), which facilitate seeing the energy release per logarithmic energy. Solid lines indicate the total disk spectra, and contributions from inner ($1.26r_g < r < 7r_g$), middle ($7r_g < r < 400r_g$), and outer parts ($400r_g < r$) are plotted separately with either dotted or broken lines. The distance and mass are assumed to be 1 kpc and 1 $M_\odot$, respectively. The Eddington luminosity is assumed, and $T_{col}/T_{eff} = 1$.

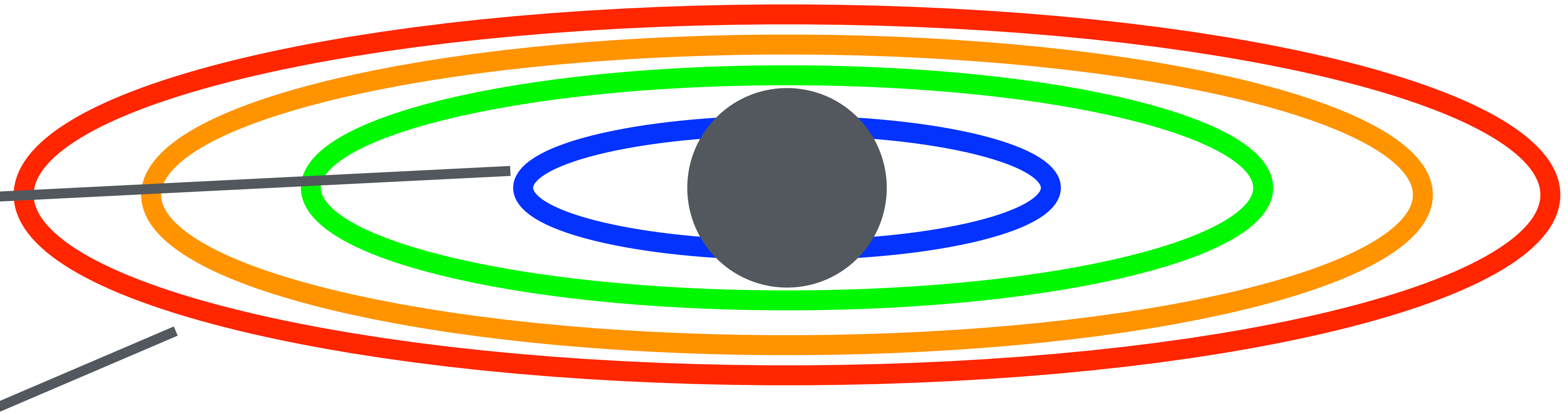

The accretion disk is divided into rings, each one a black body with increasing peak temperature with decreasing distance from the black hole.

Peak temperature → matter closest to the BH, *but*…

Color temperature is greater than the effective one, because of Comptonization: hardening factor $f \sim 1.7 - 2.0$, depending on the accretion rate (Shimura & Takahara 1995).

Spectrum of the accretion disk: multicolour black body (Mitsuda et al. 1984)

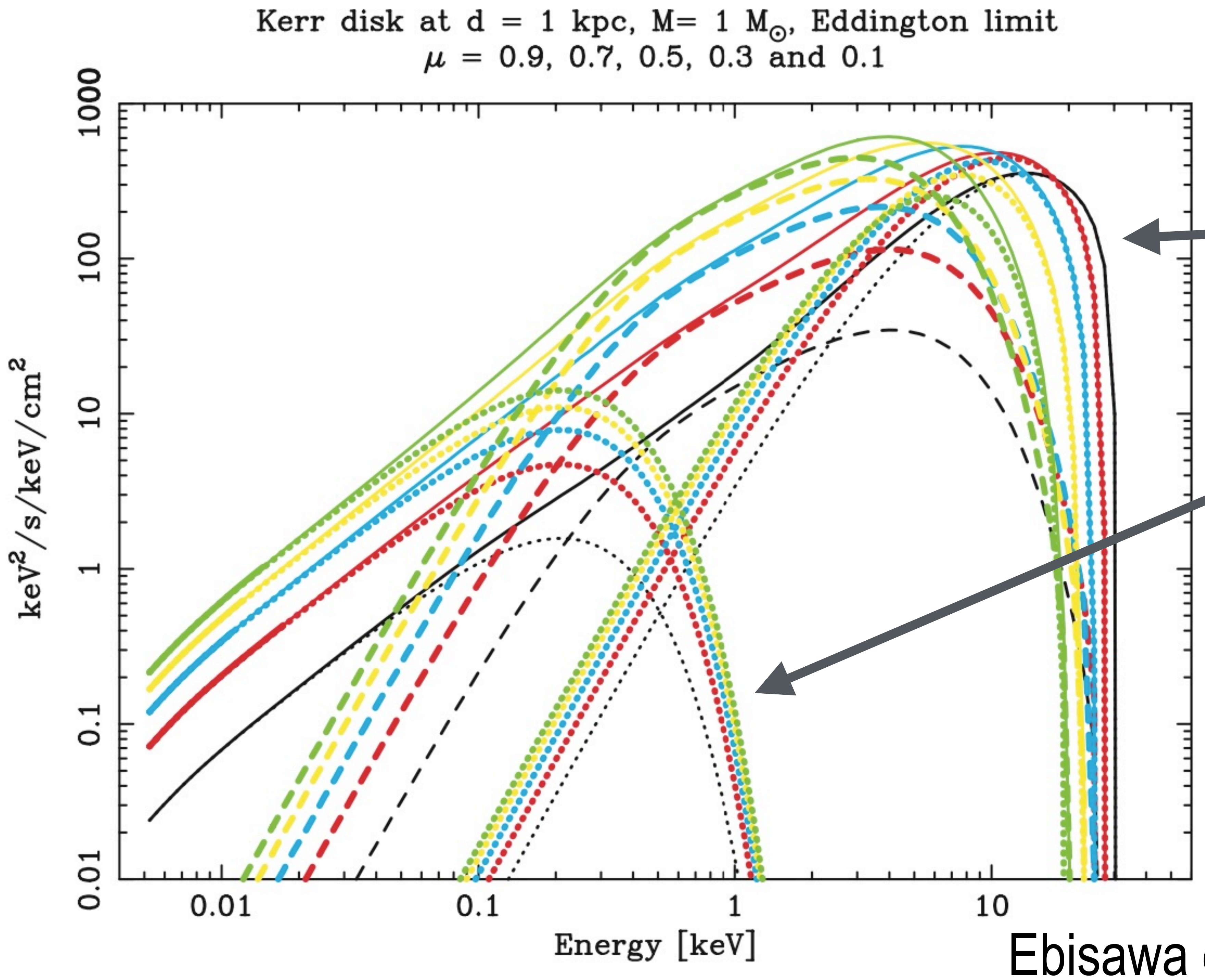

Ebisawa et al. (2003)

FIG. 2.—Kerr accretion disk spectra with an extreme angular momentum ($a = 0.998$), observed at the inclination angle $\mu \equiv \cos i = 0.9$ (*green*; near face-on), 0.7 (*yellow*), 0.5 (*cyan*), 0.3 (*red*), and 0.1 (*black*; near edge-on). Note the units of the ordinate (keV^2 s^{-1} keV^{-1} cm^{-2}), which facilitate seeing the energy release per logarithmic energy. Solid lines indicate the total disk spectra, and contributions from inner ($1.26r_g < r < 7r_g$), middle ($7r_g < r < 400r_g$), and outer parts ($400r_g < r$) are plotted separately with either dotted or broken lines. The distance and mass are assumed to be 1 kpc and 1 $M_\odot$, respectively. The Eddington luminosity is assumed, and $T_{\rm col}/T_{\rm eff} = 1$.

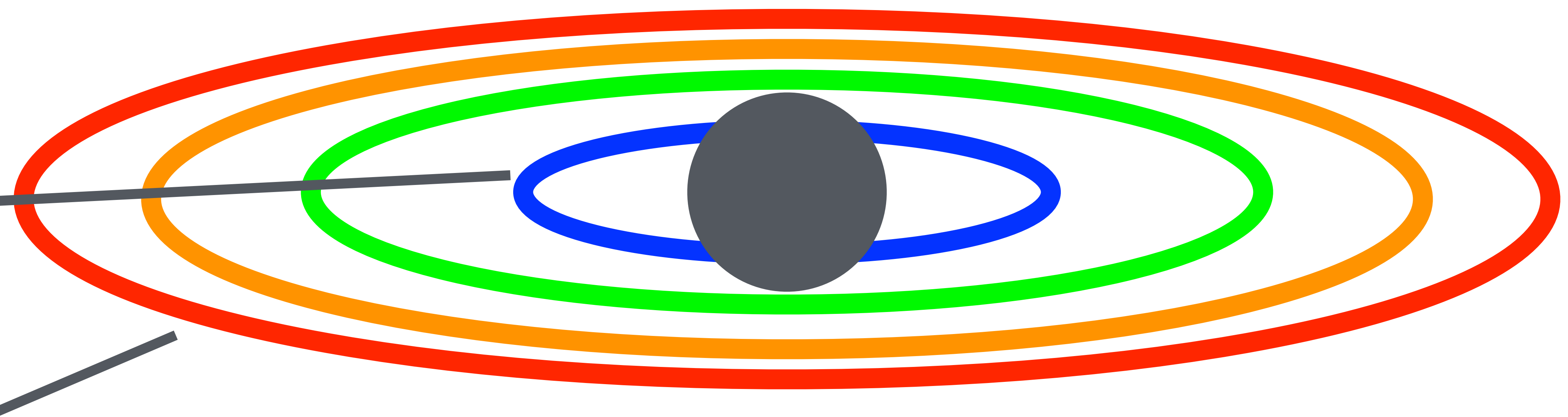

The accretion disk is divided into rings, each one a black body with increasing peak temperature with decreasing distance from the black hole.

Peak temperature → matter closest to the BH, *but*…

Color temperature is greater than the effective one, because of Comptonization: hardening factor $f \sim 1.7 - 2.0$, depending on the accretion rate (Shimura & Takahara 1995).

Correction for effective location $\varsigma \sim 0.412$ (boundary conditions, Kubota et al. 1998)

Spectrum of the accretion disk: multicolour black body (Mitsuda et al. 1984)

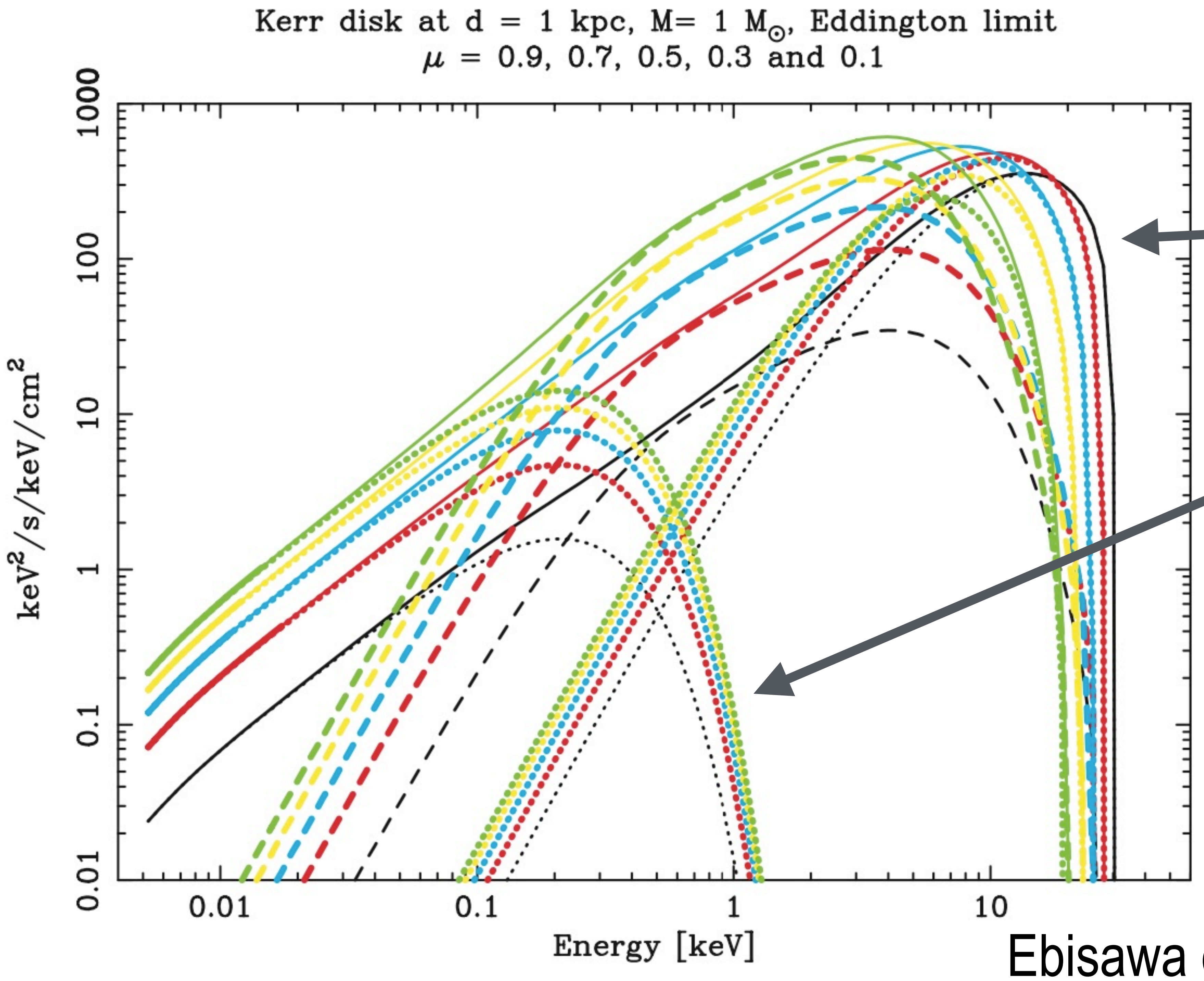

Ebisawa et al. (2003)

FIG. 2.—Kerr accretion disk spectra with an extreme angular momentum ($a = 0.998$), observed at the inclination angle $\mu \equiv \cos i = 0.9$ (*green*; near face-on), 0.7 (*yellow*), 0.5 (*cyan*), 0.3 (*red*), and 0.1 (*black*; near edge-on). Note the units of the ordinate (keV^2 s^{-1} keV^{-1} cm^{-2}), which facilitate seeing the energy release per logarithmic energy. Solid lines indicate the total disk spectra, and contributions from inner ($1.26r_g < r < 7r_g$), middle ($7r_g < r < 400r_g$), and outer parts ($400r_g < r$) are plotted separately with either dotted or broken lines. The distance and mass are assumed to be 1 kpc and 1 $M_\odot$, respectively. The Eddington luminosity is assumed, and $T_{\rm col}/T_{\rm eff} = 1$.

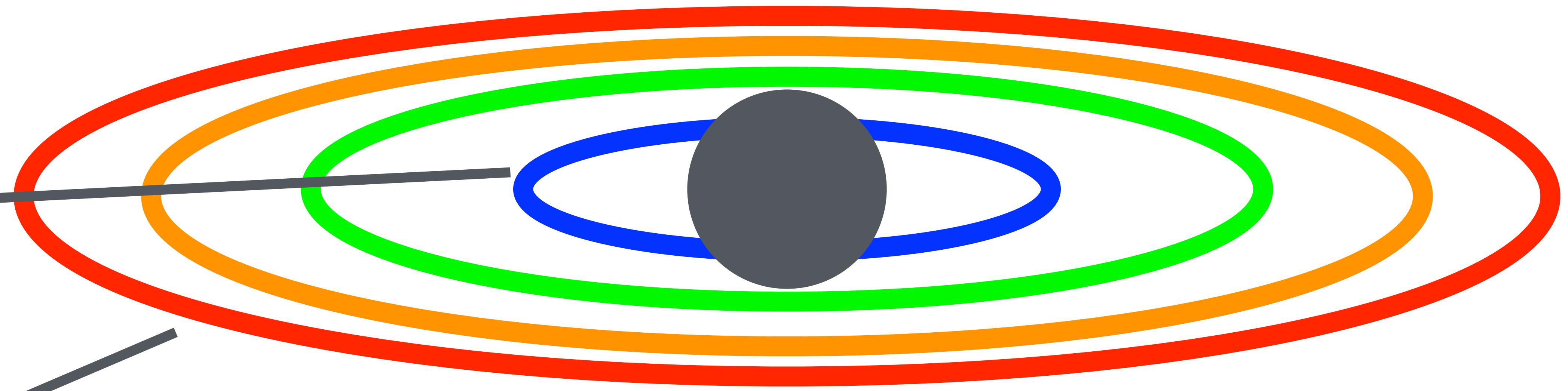

The accretion disk is divided into rings, each one a black body with increasing peak temperature with decreasing distance from the black hole.

Peak temperature → matter closest to the BH, *but*…

Color temperature is greater than the effective one, because of Comptonization: hardening factor $f \sim 1.7 - 2.0$, depending on the accretion rate (Shimura & Takahara 1995).

Correction for effective location $\varsigma \sim 0.412$ (boundary conditions, Kubota et al. 1998)

Two ways to measure $r_{\rm in}$ (both based on the Stefan-Boltzmann law):

Peak temperature and disk flux;
Normalisation of **`diskbb`** model in **`XSPEC`**

Spectrum of the accretion disk: multicolour black body (Mitsuda et al. 1984)

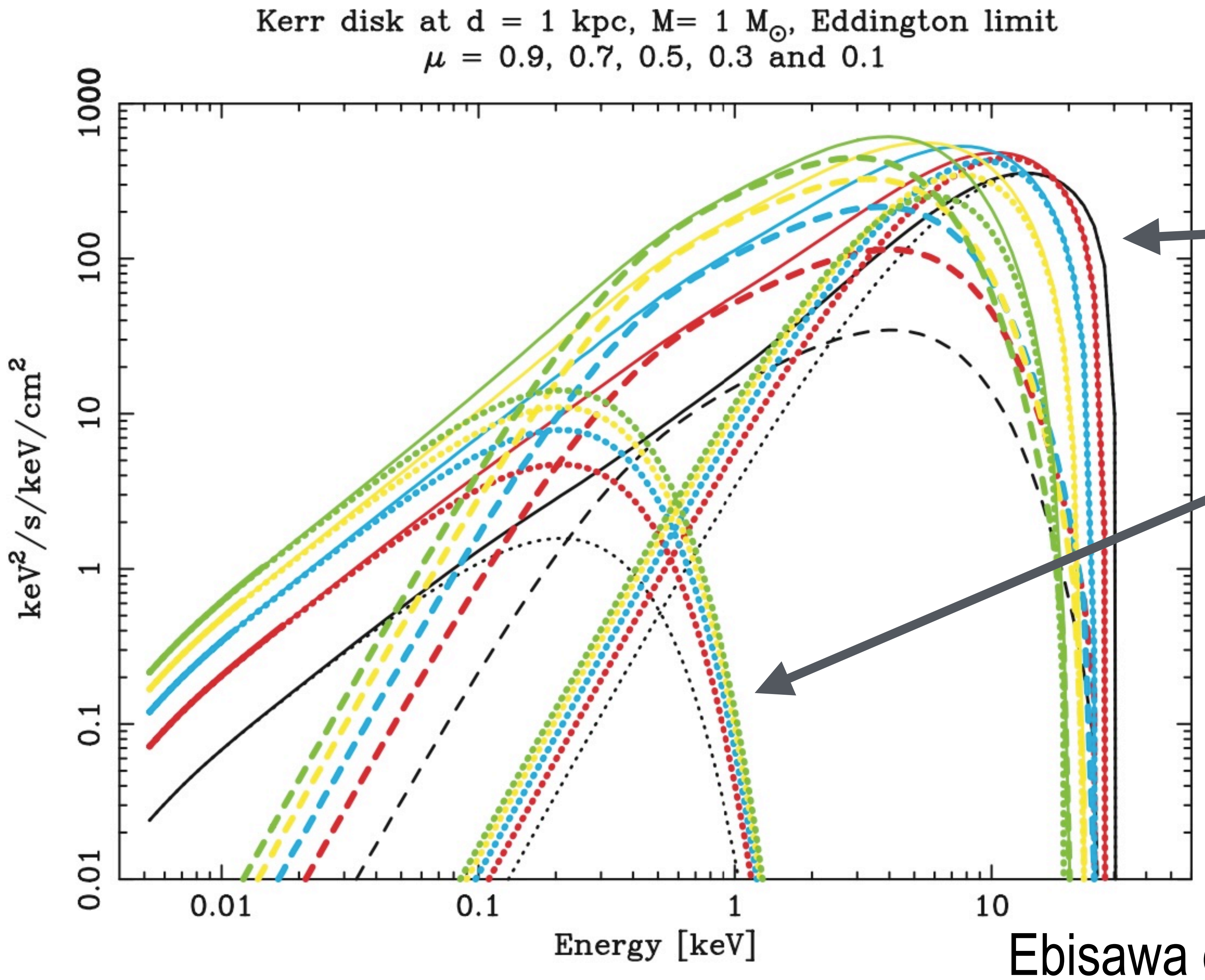

Ebisawa et al. (2003)

FIG. 2.—Kerr accretion disk spectra with an extreme angular momentum ($a = 0.998$), observed at the inclination angle $\mu \equiv \cos i = 0.9$ (*green*; near face-on), 0.7 (*yellow*), 0.5 (*cyan*), 0.3 (*red*), and 0.1 (*black*; near edge-on). Note the units of the ordinate (keV^2 s^{-1} keV^{-1} cm^{-2}), which facilitate seeing the energy release per logarithmic energy. Solid lines indicate the total disk spectra, and contributions from inner ($1.26r_g < r < 7r_g$), middle ($7r_g < r < 400r_g$), and outer parts ($400r_g < r$) are plotted separately with either dotted or broken lines. The distance and mass are assumed to be 1 kpc and 1 $M_\odot$, respectively. The Eddington luminosity is assumed, and $T_{\rm col}/T_{\rm eff} = 1$.

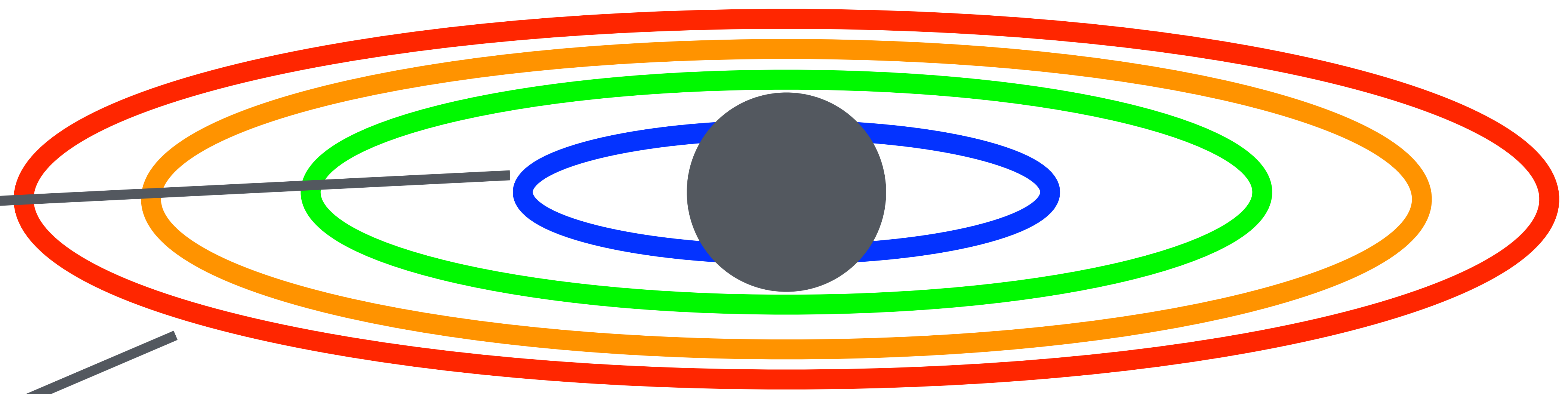

The accretion disk is divided into rings, each one a black body with increasing peak temperature with decreasing distance from the black hole.

Peak temperature → matter closest to the BH, *but*…

Color temperature is greater than the effective one, because of Comptonization: hardening factor $f \sim 1.7 - 2.0$, depending on the accretion rate (Shimura & Takahara 1995).

Correction for effective location $\varsigma \sim 0.412$ (boundary conditions, Kubota et al. 1998)

Two ways to measure $r_{\rm in}$ (both based on the Stefan-Boltzmann law):

$$r_{\rm in} = \varsigma f^2 \frac{d}{\sqrt{\cos i}} \sqrt{\frac{F_{\rm disk}}{2\sigma T_{\rm in}^4}}$$

Peak temperature and disk flux;
Normalisation of `diskbb` model in `XSPEC`

Stefan-Boltzmann constant

Spectrum of the accretion disk: multicolour black body (Mitsuda et al. 1984)

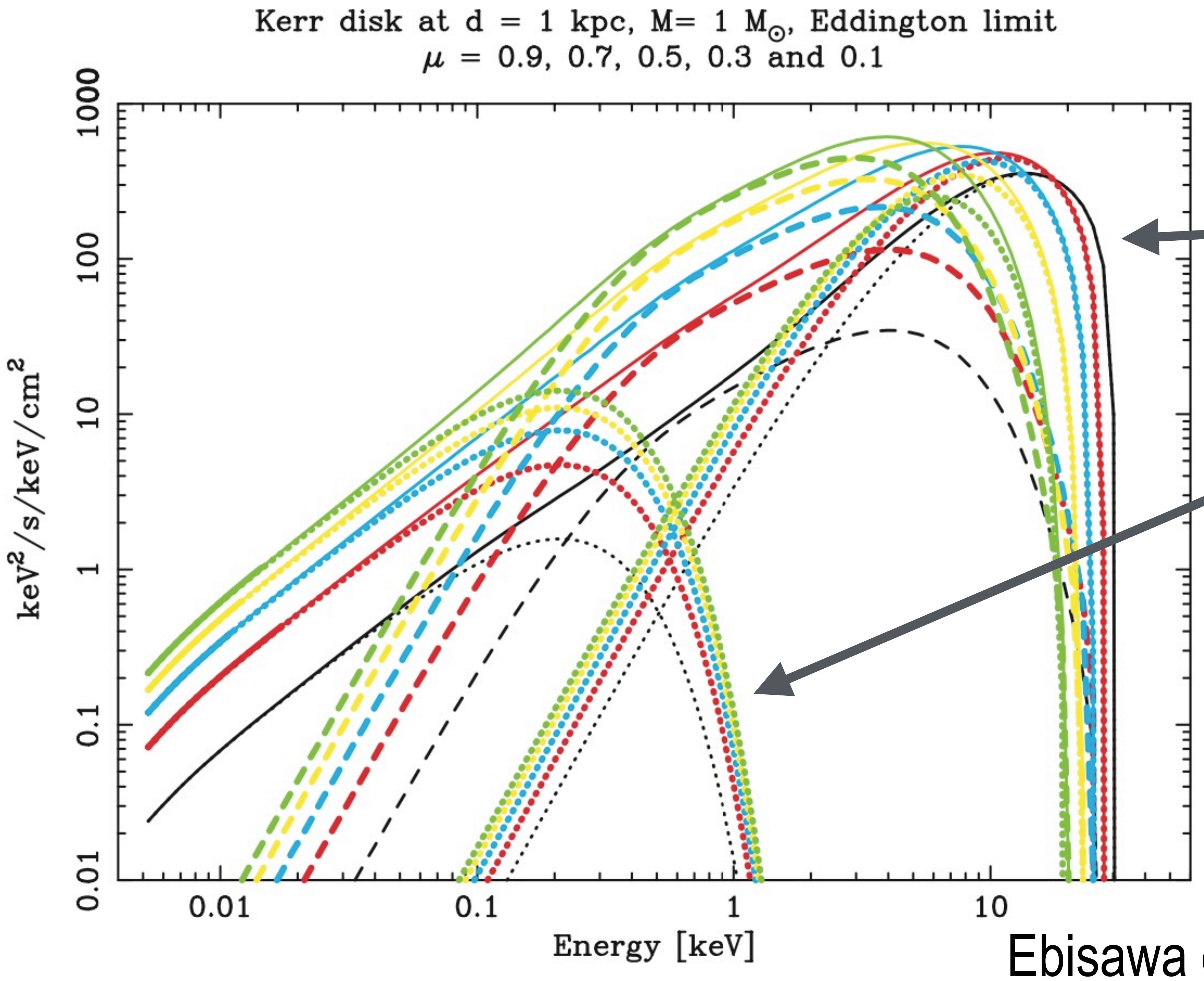

Ebisawa et al. (2003)

FIG. 2.—Kerr accretion disk spectra with an extreme angular momentum ($a = 0.998$), observed at the inclination angle $\mu \equiv \cos i = 0.9$ (*green*; near face-on), 0.7 (*yellow*), 0.5 (*cyan*), 0.3 (*red*), and 0.1 (*black*; near edge-on). Note the units of the ordinate (keV^2 s^{-1} keV^{-1} cm^{-2}), which facilitate seeing the energy release per logarithmic energy. Solid lines indicate the total disk spectra, and contributions from inner ($1.26r_g < r < 7r_g$), middle ($7r_g < r < 400r_g$), and outer parts ($400r_g < r$) are plotted separately with either dotted or broken lines. The distance and mass are assumed to be 1 kpc and 1 $M_\odot$, respectively. The Eddington luminosity is assumed, and $T_{\rm col}/T_{\rm eff} = 1$.

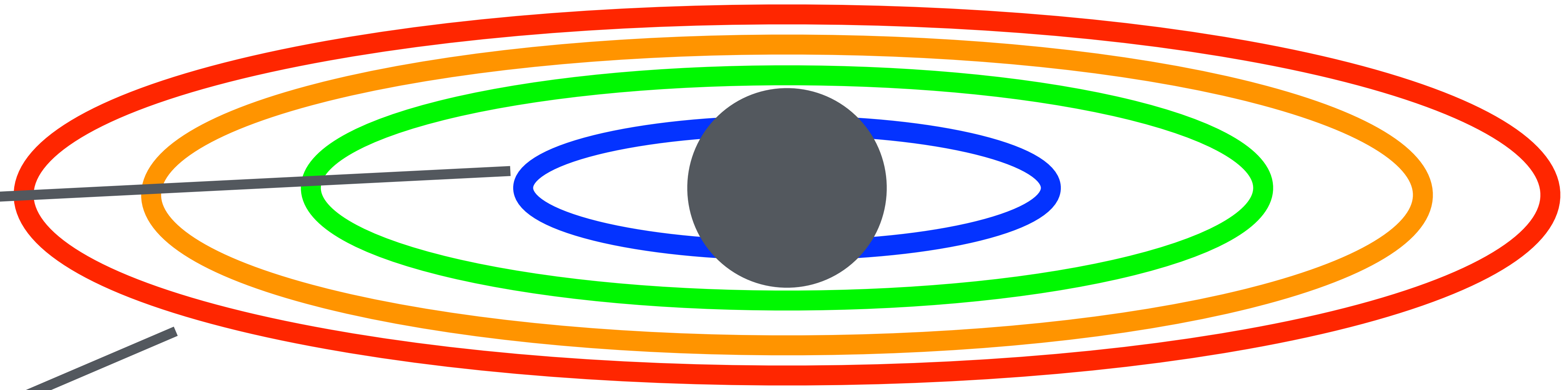

The accretion disk is divided into rings, each one a black body with increasing peak temperature with decreasing distance from the black hole.

Peak temperature → matter closest to the BH, *but*…

Color temperature is greater than the effective one, because of Comptonization: hardening factor $f \sim 1.7 - 2.0$, depending on the accretion rate (Shimura & Takahara 1995).

Correction for effective location $\varsigma \sim 0.412$ (boundary conditions, Kubota et al. 1998)

Two ways to measure $r_{\rm in}$ (both based on the Stefan-Boltzmann law):

$$r_{\rm in} = \varsigma f^2 \frac{d}{\sqrt{\cos i}} \sqrt{\frac{F_{\rm disk}}{2\sigma T_{\rm in}^4}}$$

Stefan-Boltzmann constant

Peak temperature and disk flux;
Normalisation of `diskbb` model in `XSPEC`

$$r_{\rm in} = \varsigma f^2 d_{10} \sqrt{\frac{N}{\cos i}}$$

Distance in units of 10 kpc

States of stellar-mass black holes

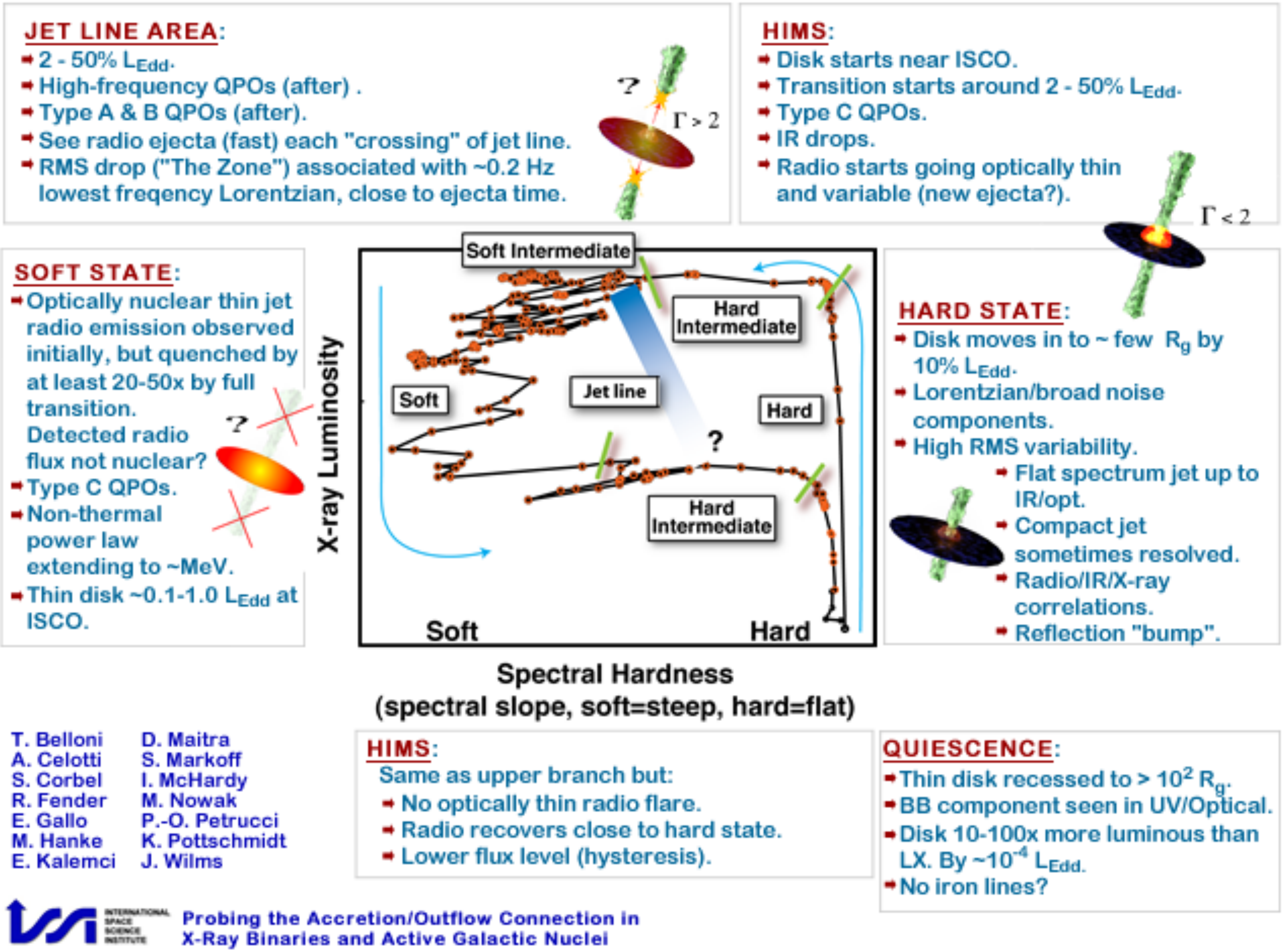

http://www.issibern.ch/teams/proaccretion/
https://www.sternwarte.uni-erlangen.de/proaccretion/

States of stellar-mass black holes

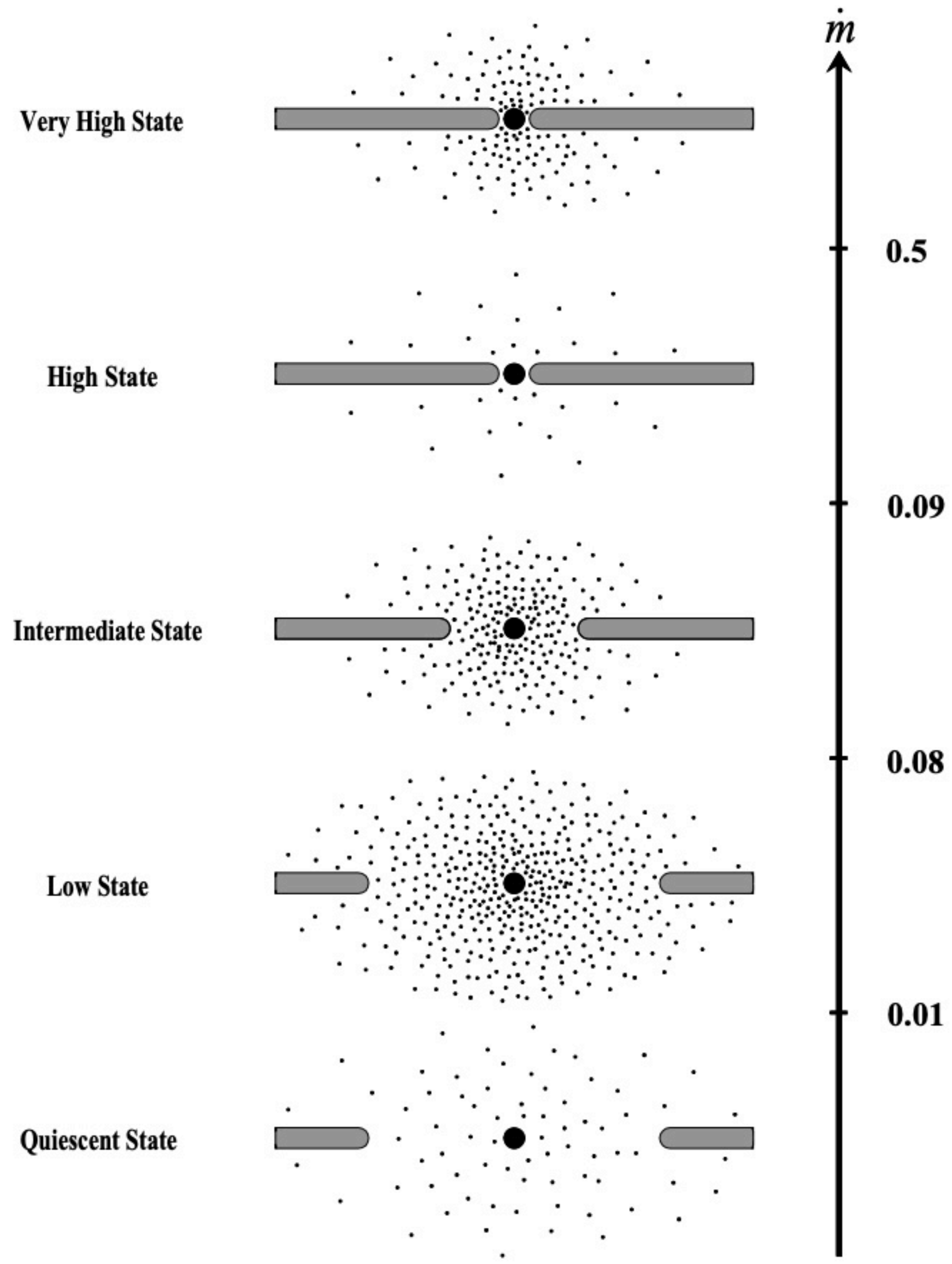

Esin et al. (1997)

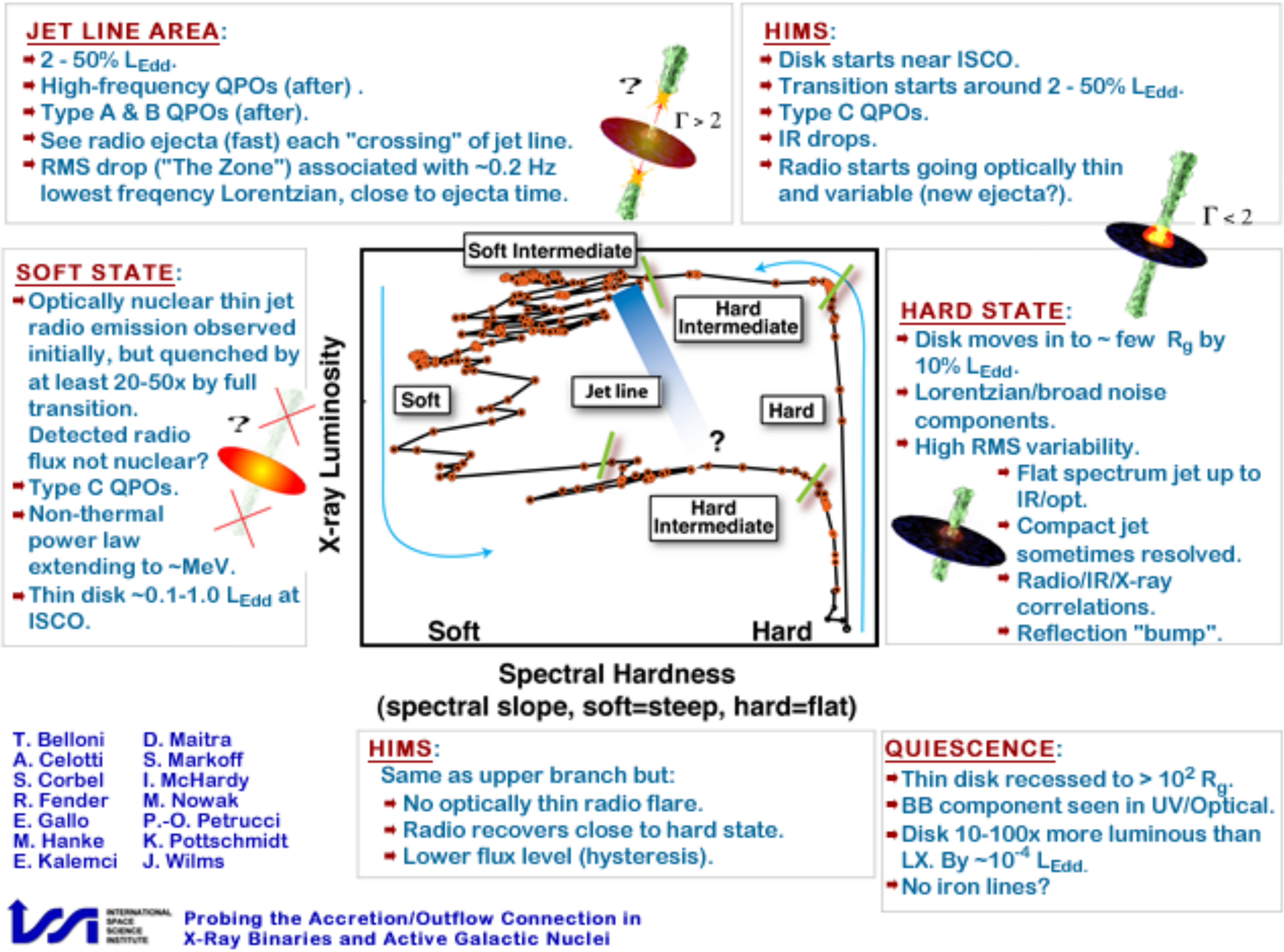

http://www.issibern.ch/teams/proaccretion/
https://www.sternwarte.uni-erlangen.de/proaccretion/

States of stellar-mass black holes

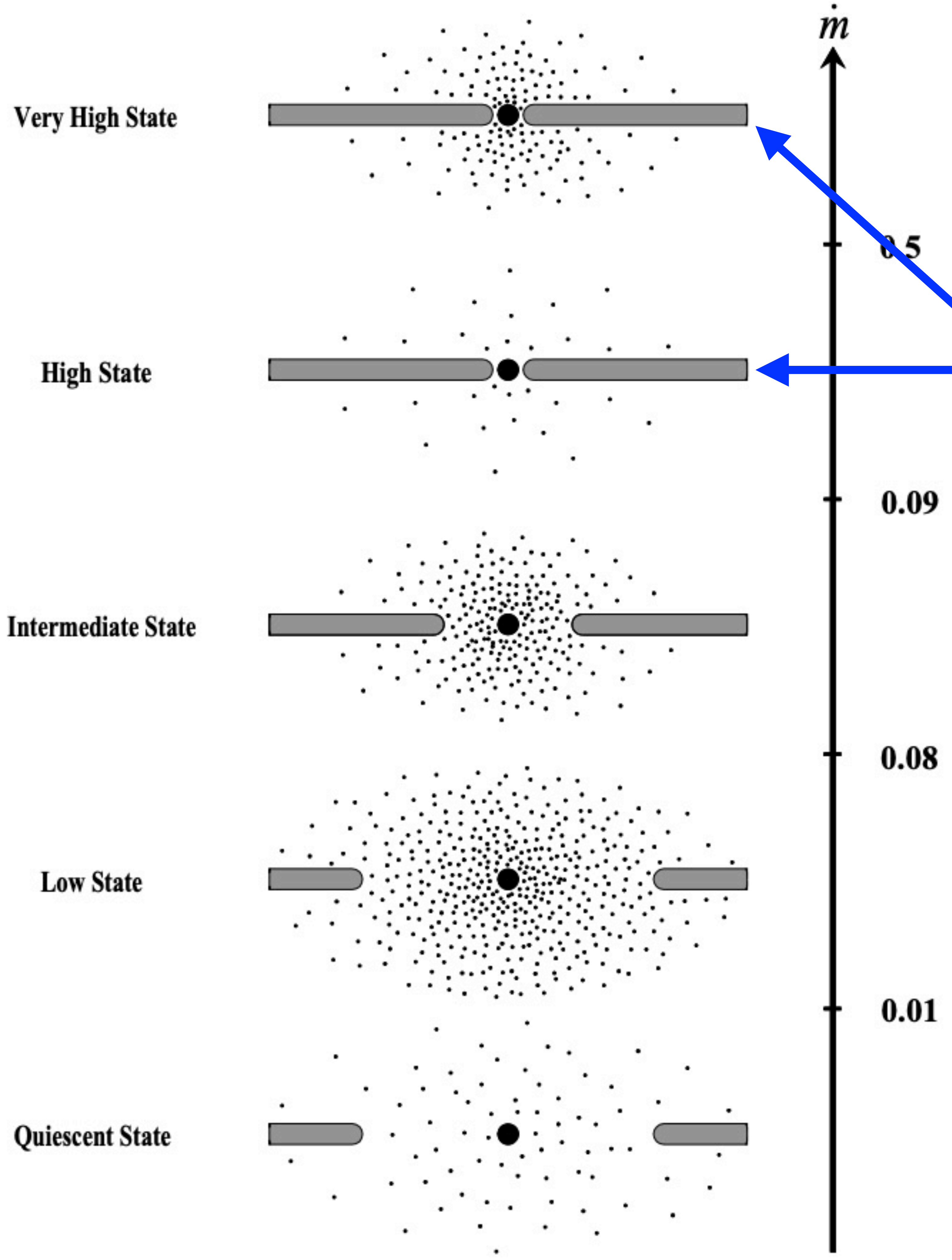

Esin et al. (1997)

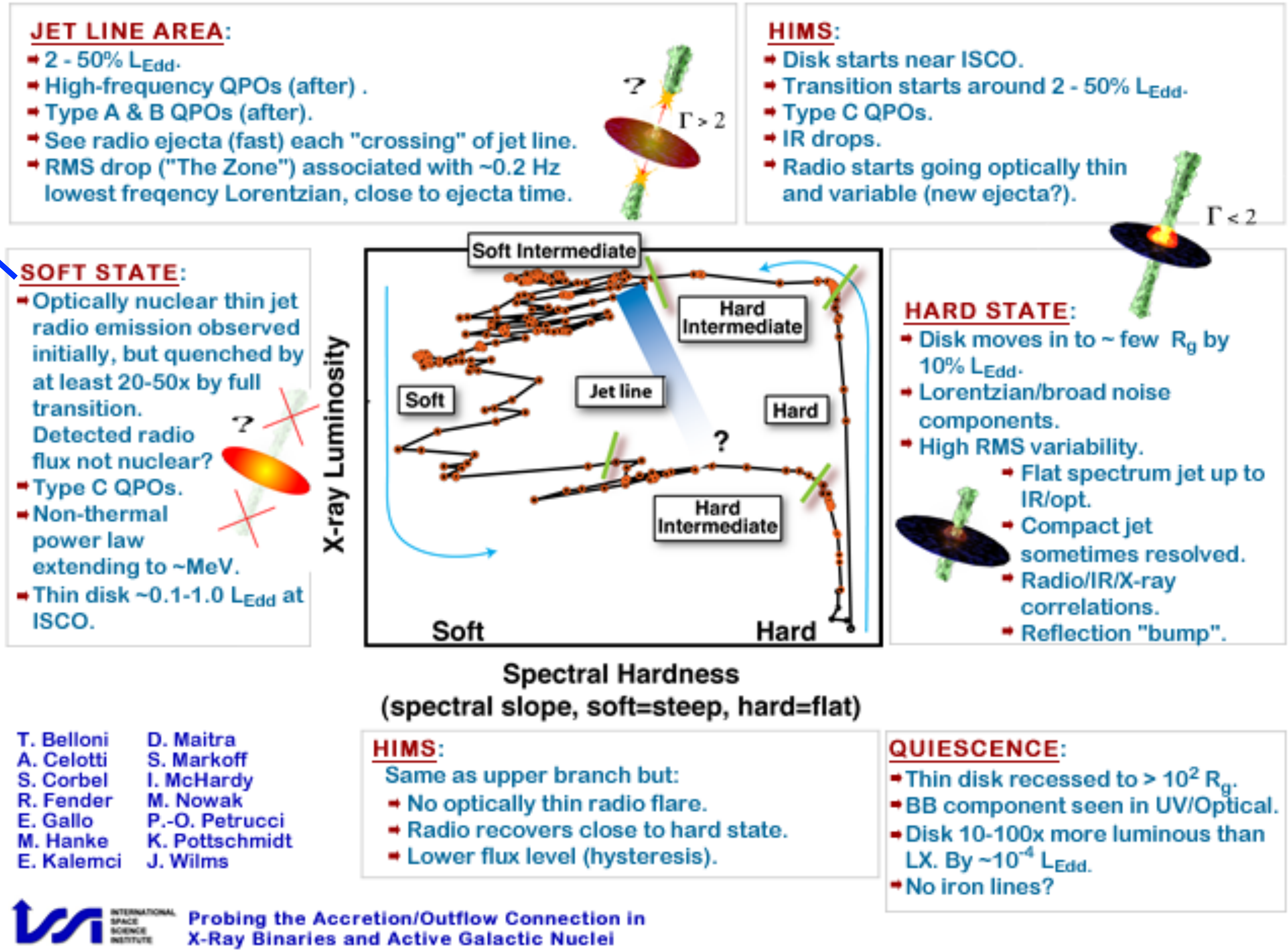

http://www.issibern.ch/teams/proaccretion/
https://www.sternwarte.uni-erlangen.de/proaccretion/

States of stellar-mass black holes

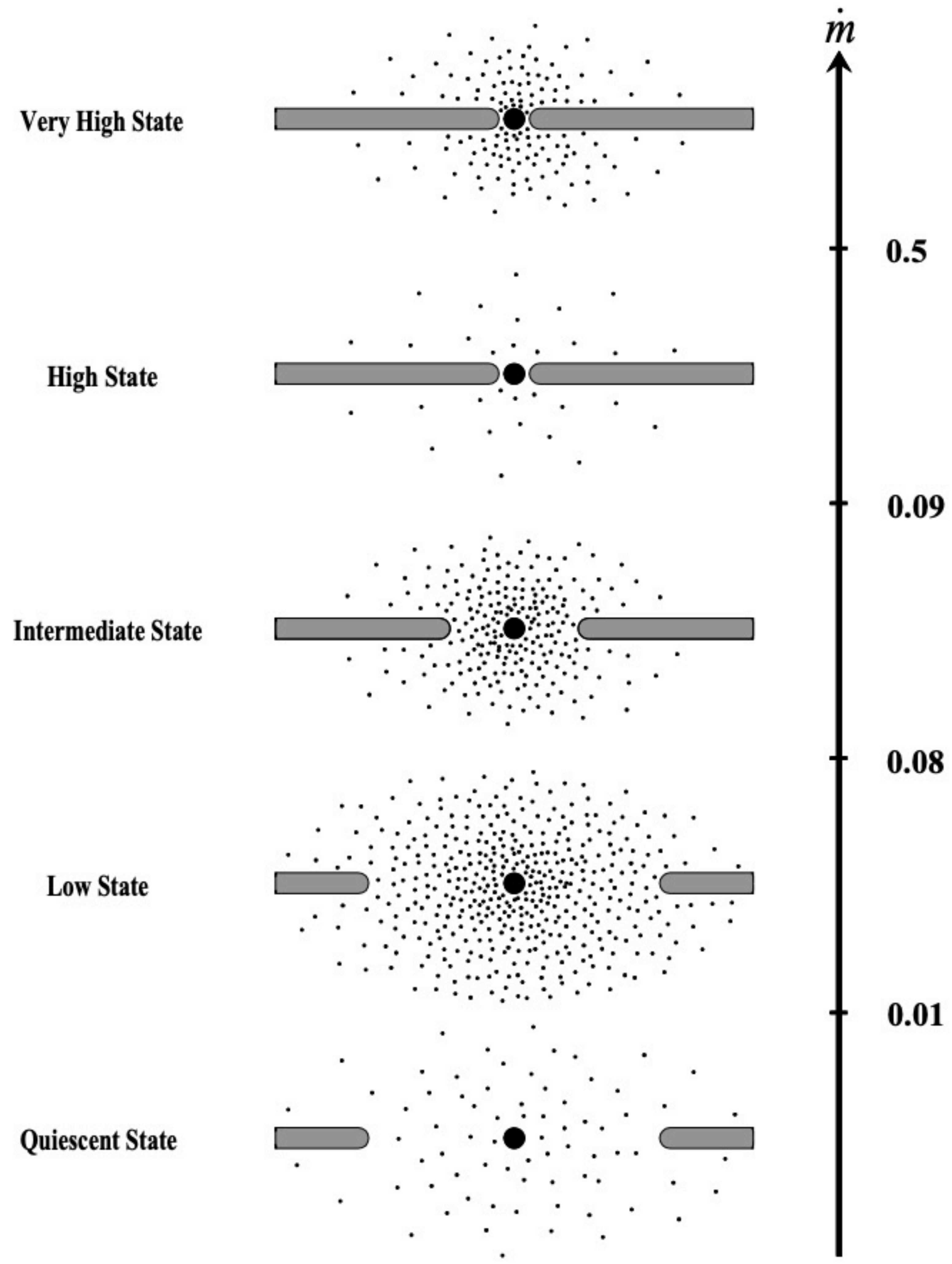

Esin et al. (1997)

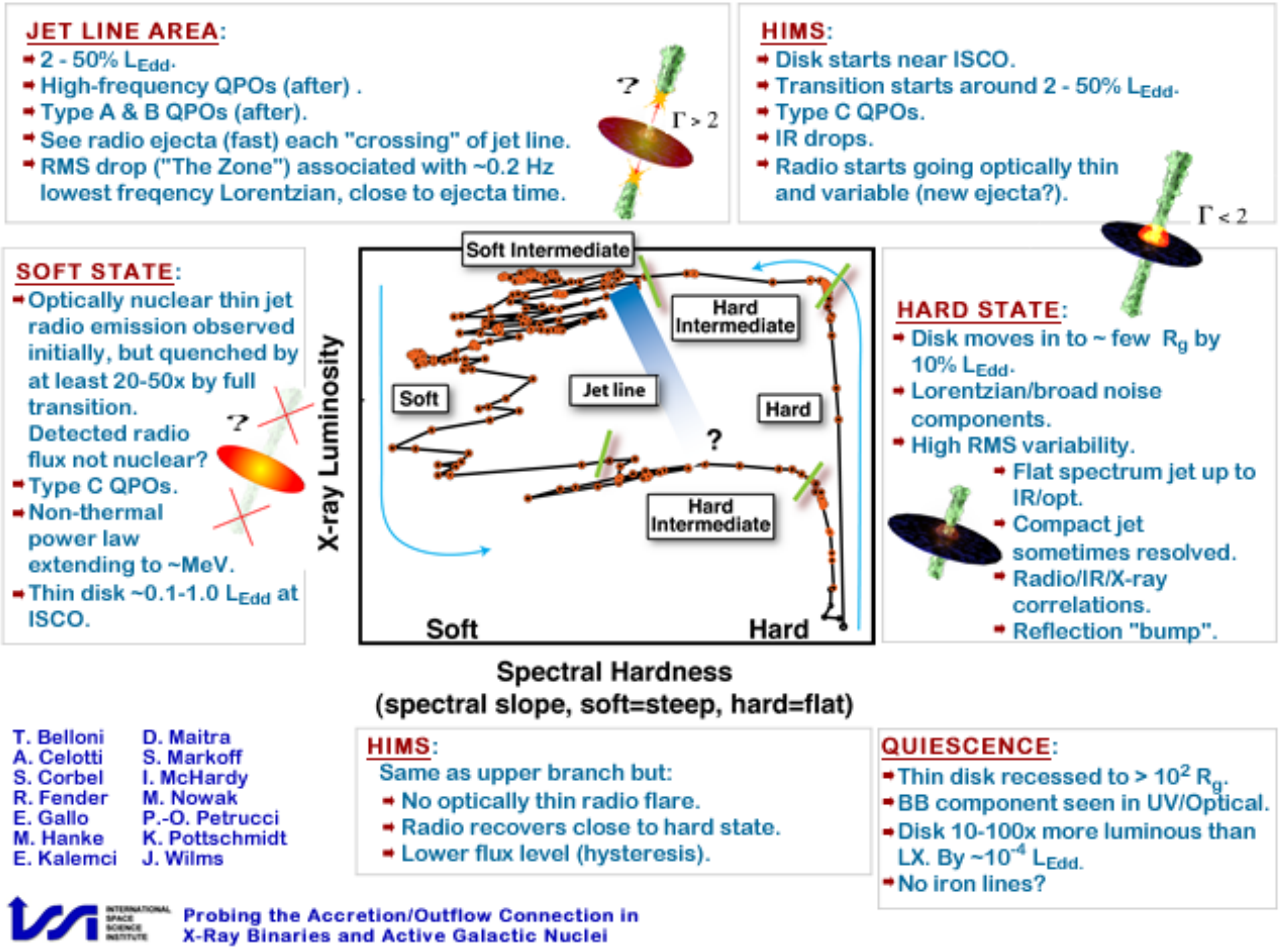

http://www.issibern.ch/teams/proaccretion/
https://www.sternwarte.uni-erlangen.de/proaccretion/

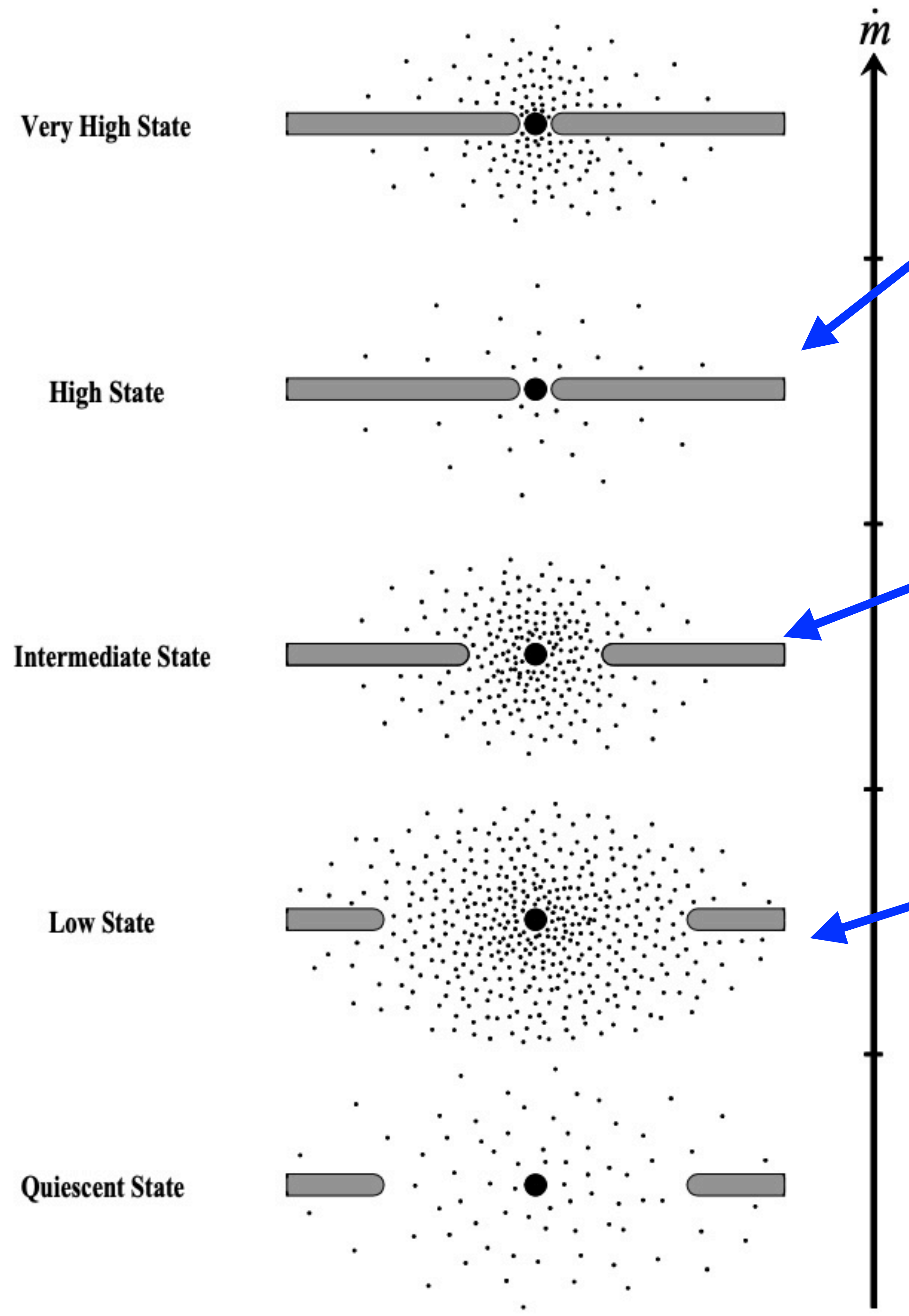

Esin et al. (1997)

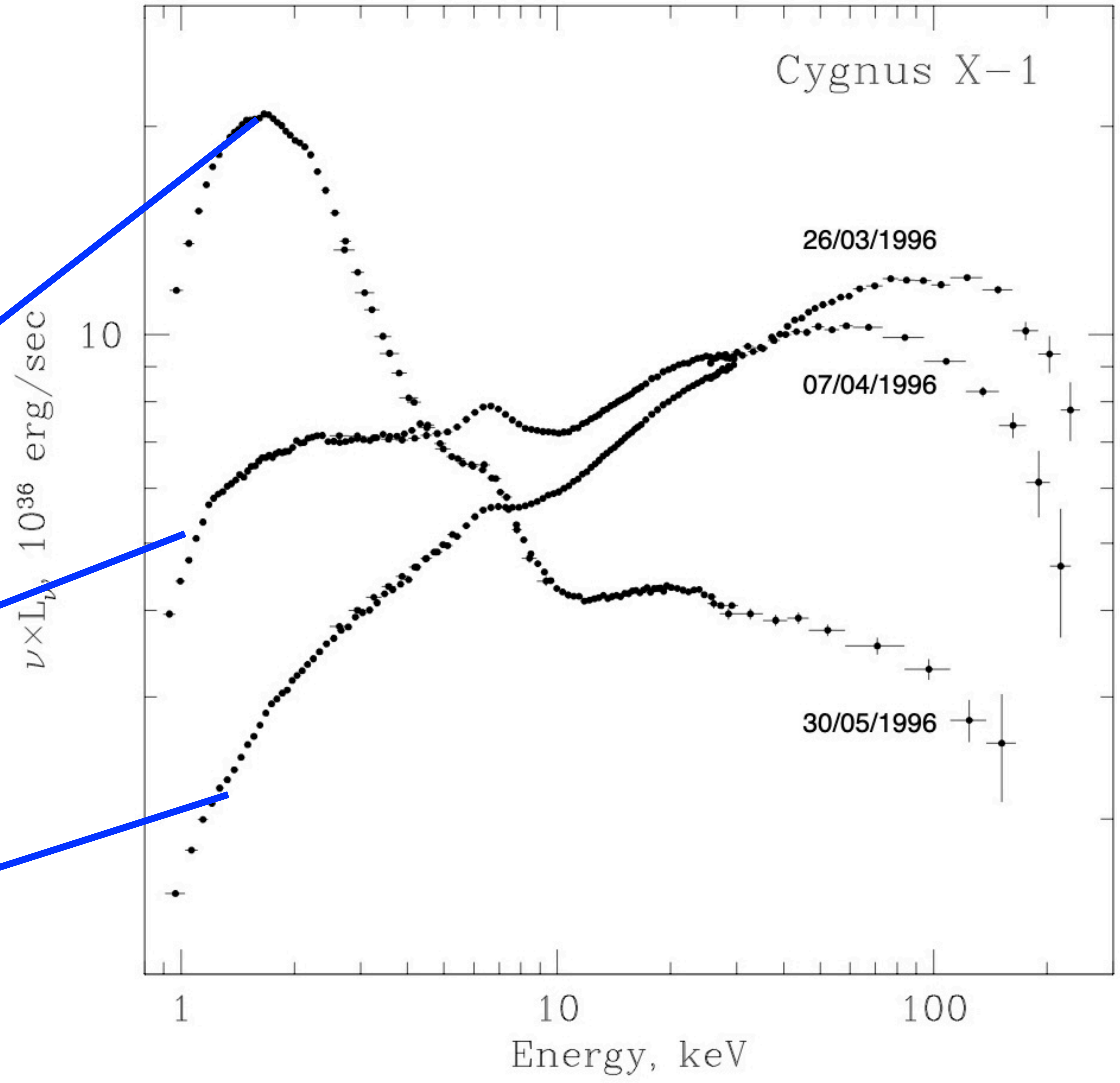

Meyer et al. (2000)

Fig. 1. Transition from the hard spectrum on 26/3/1996 to a soft spectrum on 30/5/1996, observed for Cygnus X-1 (from M. Gilfanov, E. Churazov, M.G. Revnivtsev, in preparation)

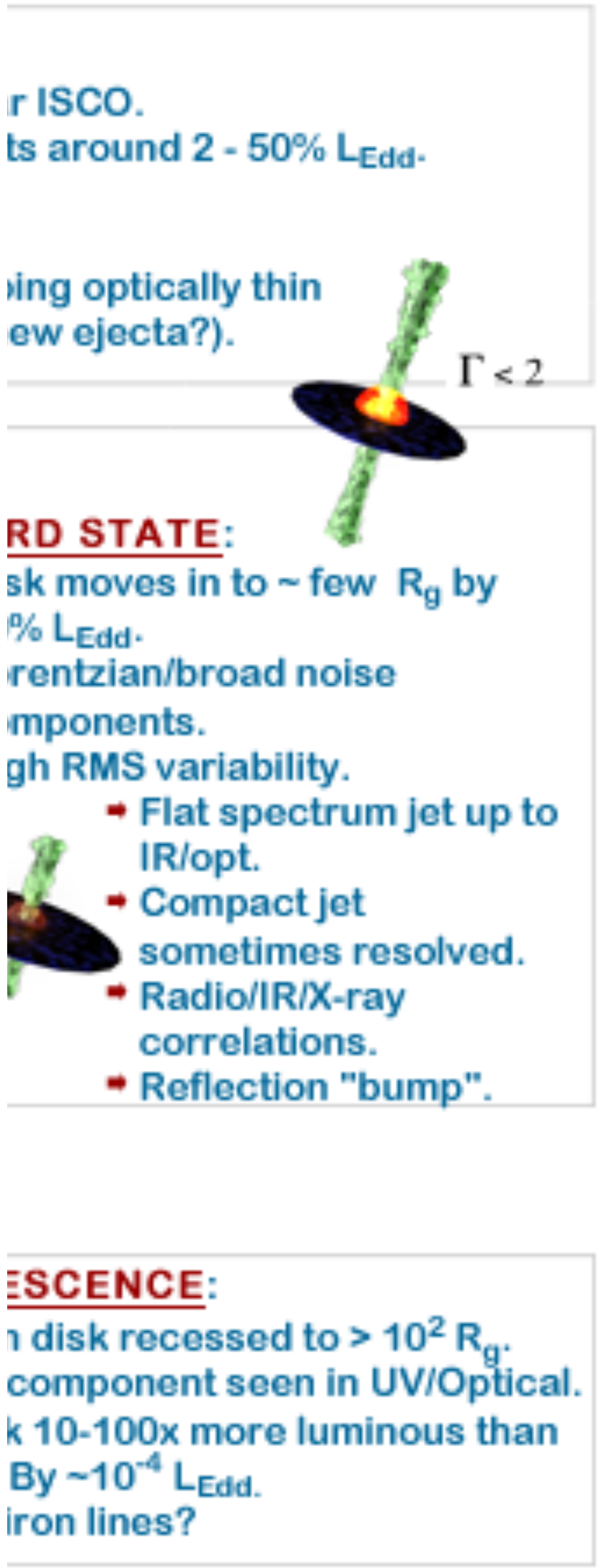

ams/proaccretion/
.de/proaccretion/

Issues in data collection

- Searching in all the literature;
- Reference quantities (BH mass, distance, inclination, spin) changed during years: once selected the best data set, there is need to make all data homogeneous before comparing them;
- It’s not easy:
    - many authors did not publish all the necessary information (adopted distance and inclination were often missing);
    - upper limits not recognized, missing measurement errors (for fluxes we assumed ~10%);
    - missing measurement units;
    - plain errors, typos;
- Nevertheless, it is a better approach than download and reanalyse raw data, because it is possible to cover a longer time interval, use information from different X-ray satellites, and identify immediately the soft states.

Instrumental biases

How reliable is the measurement of the inner disk temperature?

Strongly dependent on the low-energy threshold of the detector.

Example: RXTE/PCA, low-energy threshold 2 keV

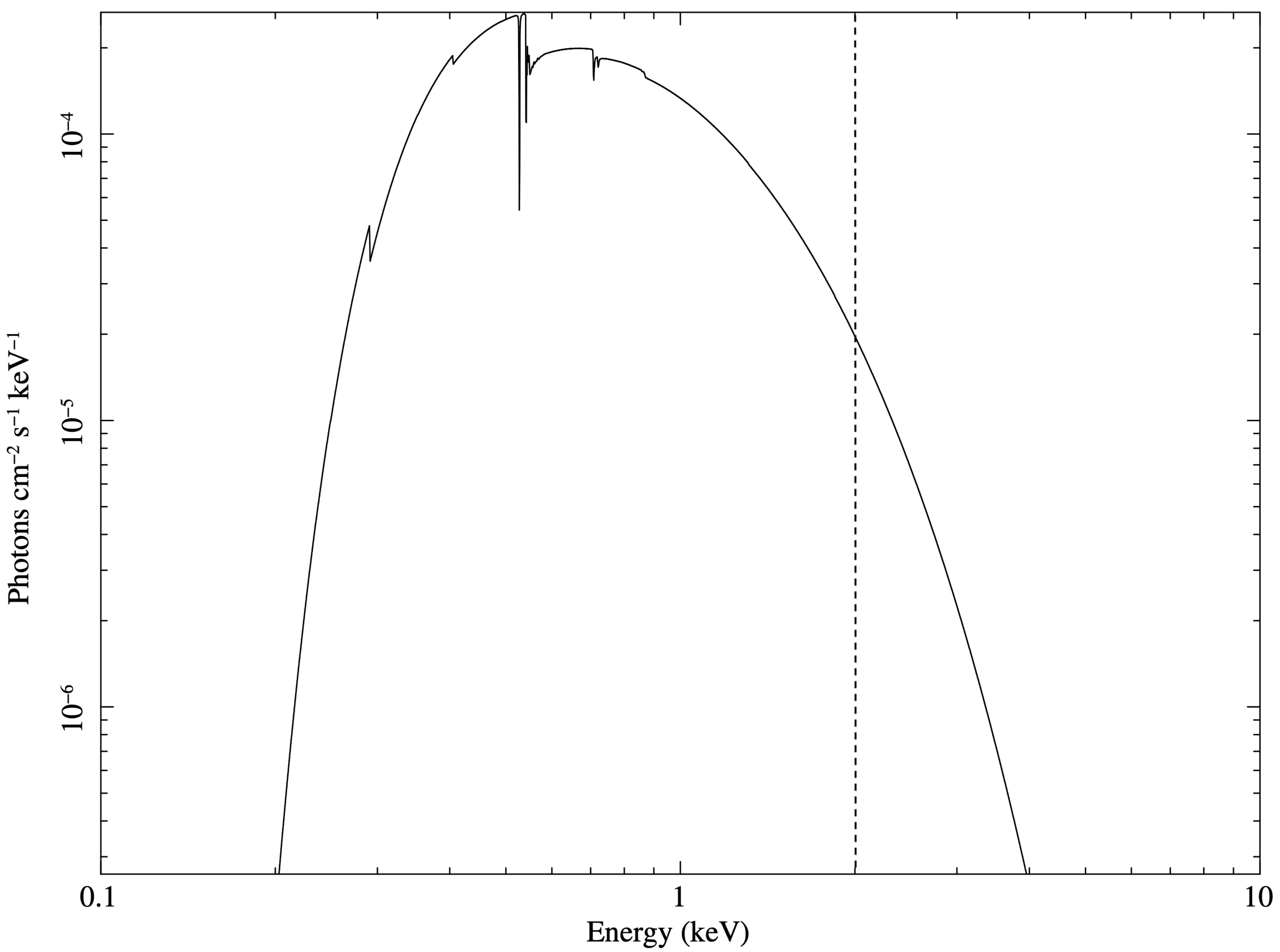

$N_H = 10^{21}\,\mathrm{cm}^{-2}$ $\quad\quad$ $T_{in} = 0.4\,\mathrm{keV}$

Instrumental biases

How reliable is the measurement of the inner disk temperature?

Strongly dependent on the low-energy threshold of the detector.

Example: RXTE/PCA, low-energy threshold 2 keV

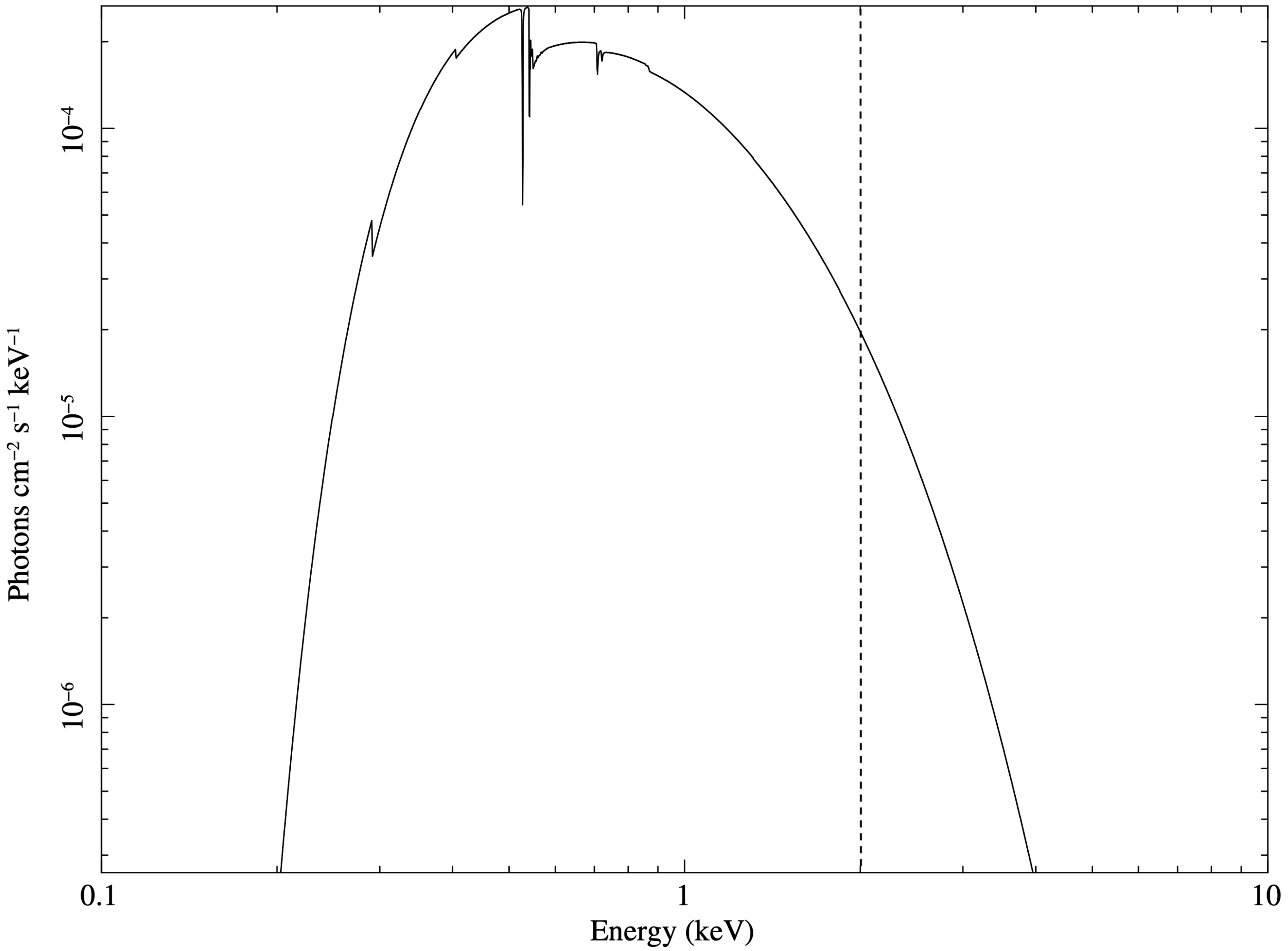

$N_H = 10^{21}\,\mathrm{cm}^{-2}$ $\qquad T_{in} = 0.4\,\mathrm{keV}$

Spectral extraction with high throughput

Example: Swift/XRT (and similar CCD detectors)

Cyg X-1

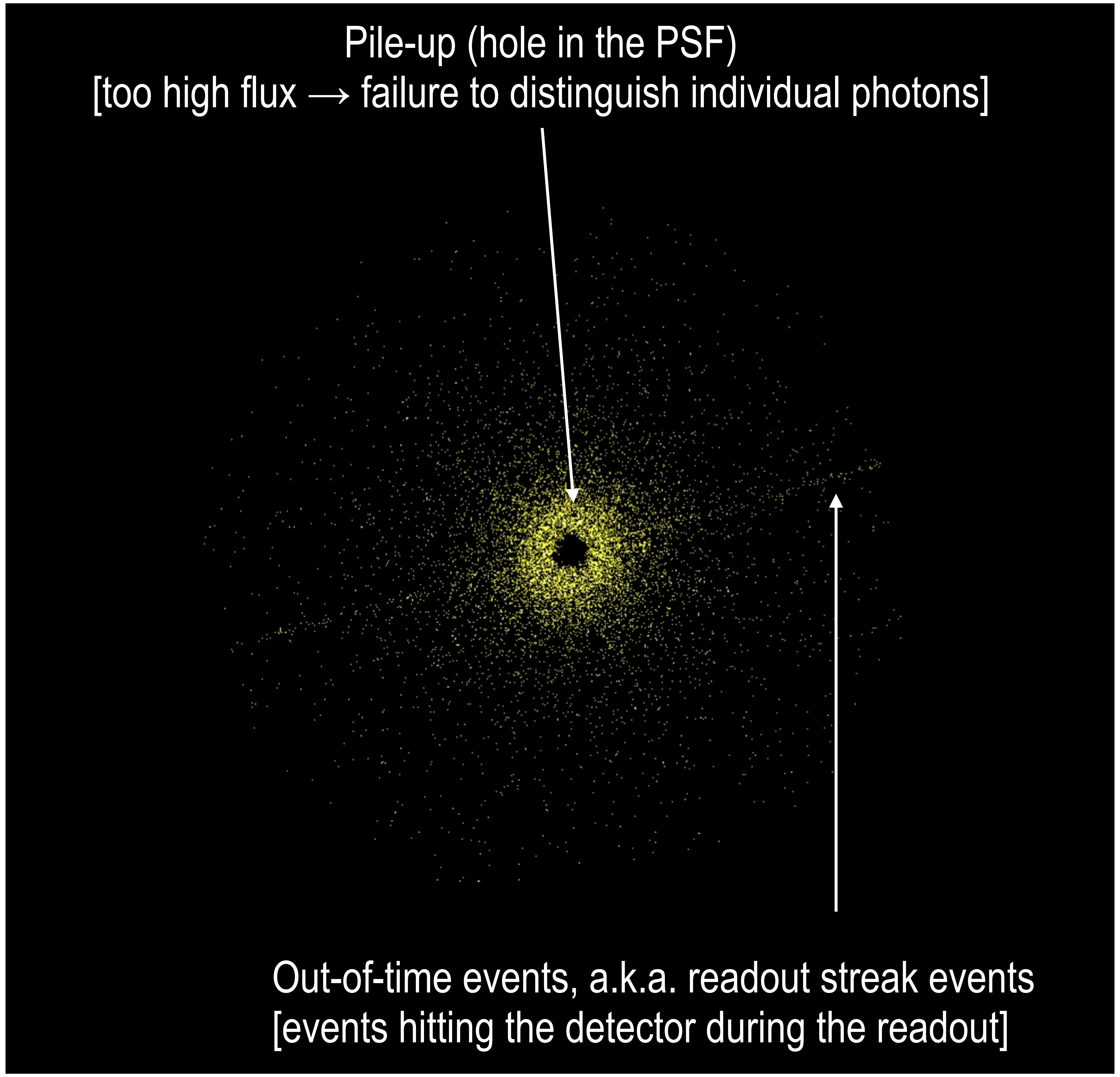

Cygnus X-1

Reference data from Miller-Jones et al. (2021)

$$M = 21.2^{+2.2}_{-2.3}\,M_\odot \rightarrow r_{\rm g} = 31 \pm 3\,{\rm km}$$

$$d = 2.22^{+0.18}_{-0.17}\,{\rm kpc}$$

$$i = 27^\circ.51^{+0.77}_{-0.57}$$

$$a = 0.9696 - 0.9985$$

$$r_{\rm isco} = (1.21 - 1.74)r_{\rm g}$$

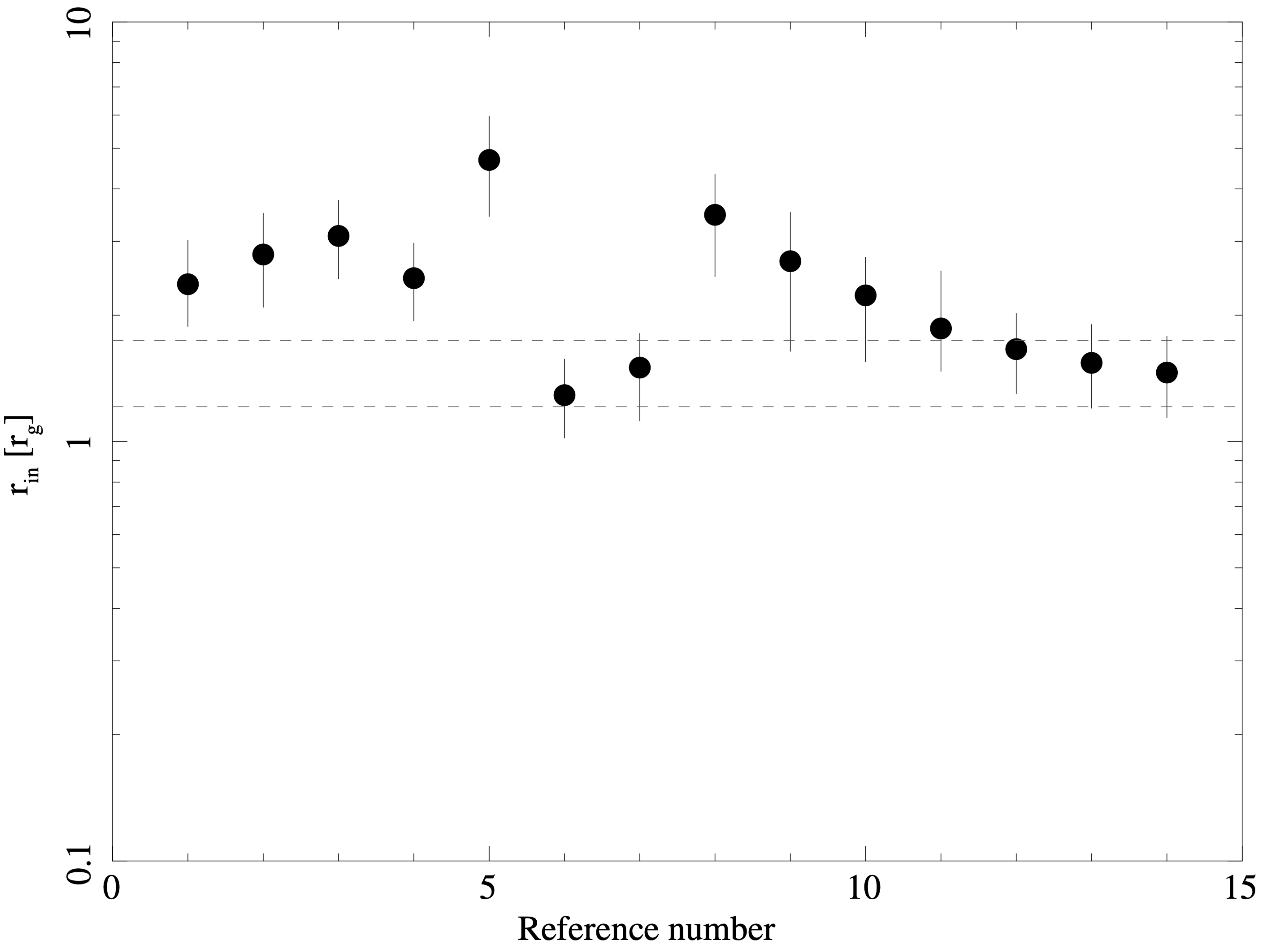

Reference number:

(1) Dotani et al. (1997)
(2) Poutanen et al. (1997)
(3-4) Cui et al. (1998)
(5) Frontera et al. (2001)
(6) Tomsick et al. (2014)
(7) Sugimoto et al. (2016)
(8-11) Walton et al. (2016)
(12-13) Kushwaha et al. (2021)
(14) Yan et al. (2021)

GRS 1915+105

Reference data from Reid & Miller-Jones (2023), Sreehari et al. (2020), Miller et al. (2013).

$$M = 11.8 \pm 0.6\, M_\odot \rightarrow r_g = 17.4 \pm 0.9\,\mathrm{km}$$

$$d = 9.4 \pm 1.0\,\mathrm{kpc}$$

$$i = 64^\circ \pm 4^\circ$$

$$a = 0.970 - 0.997$$

$$r_{\rm isco} = (1.28 - 1.74) r_g$$

Reference number:

(1-2) Taam et al. (1997)
(3) Muno et al. (1999)
(4-7) Feroci et al. (1999)
(8-10) Rao et al. (2000)
(11) Belloni et al. (2000)
(12) Zdiarski et al. (2001)
(13-22) Vadawale et al. (2001)
(23-27) Ueda et al. (2002)
(28-29) Naik et al. (2002)
(30-32) Done et al. (2004)
(33-36) Ohkawa et al. (2005)
(37-46) Rodriguez et al. (2008)
(47-50) Vierdayanti et al. (2010)
(51-54) Ueda et al. (2010)
(55-60) Rahoui et al. (2010)
(61) Neilsen et al. (2011)
(62) Miller et al. (2016)
(63-68) Mineo et al. (2017)
(69) HESS Collaboration (2018)

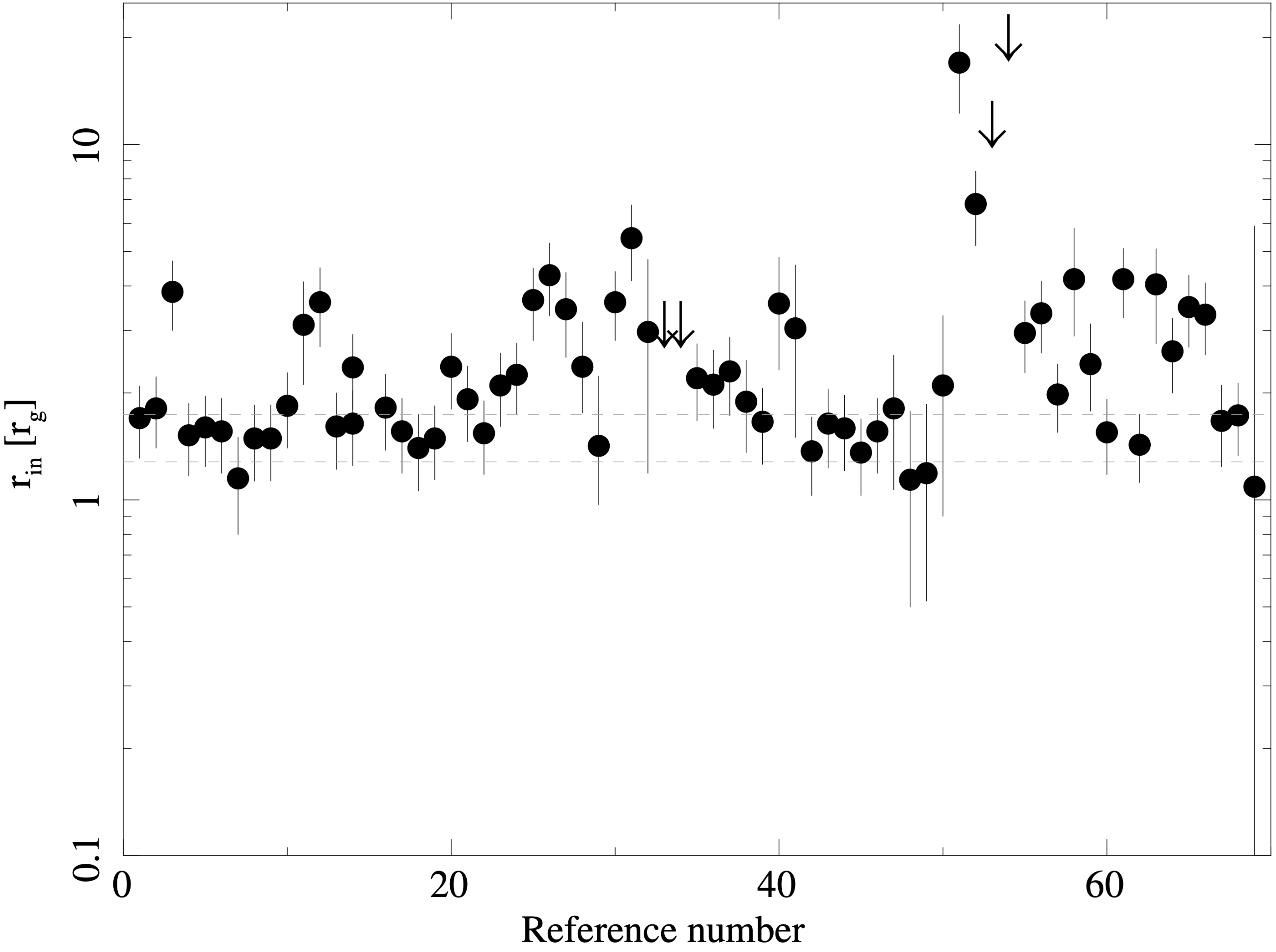

XTE J1550-564

Reference data from Orosz et al. (2011), Steiner et al. (2011)

$$M = 9.10 \pm 0.61\, M_{\odot} \rightarrow r_{\rm g} = 13.4 \pm 0.9\,{\rm km}$$

$$d = 4.38^{+0.58}_{-0.41}\,{\rm kpc}$$

$$i = 74^{\circ}.7 \pm 3^{\circ}.8$$

$$a = 0.29 - 0.62$$

$$r_{\rm isco} = (3.74 - 5.01) r_{\rm g}$$

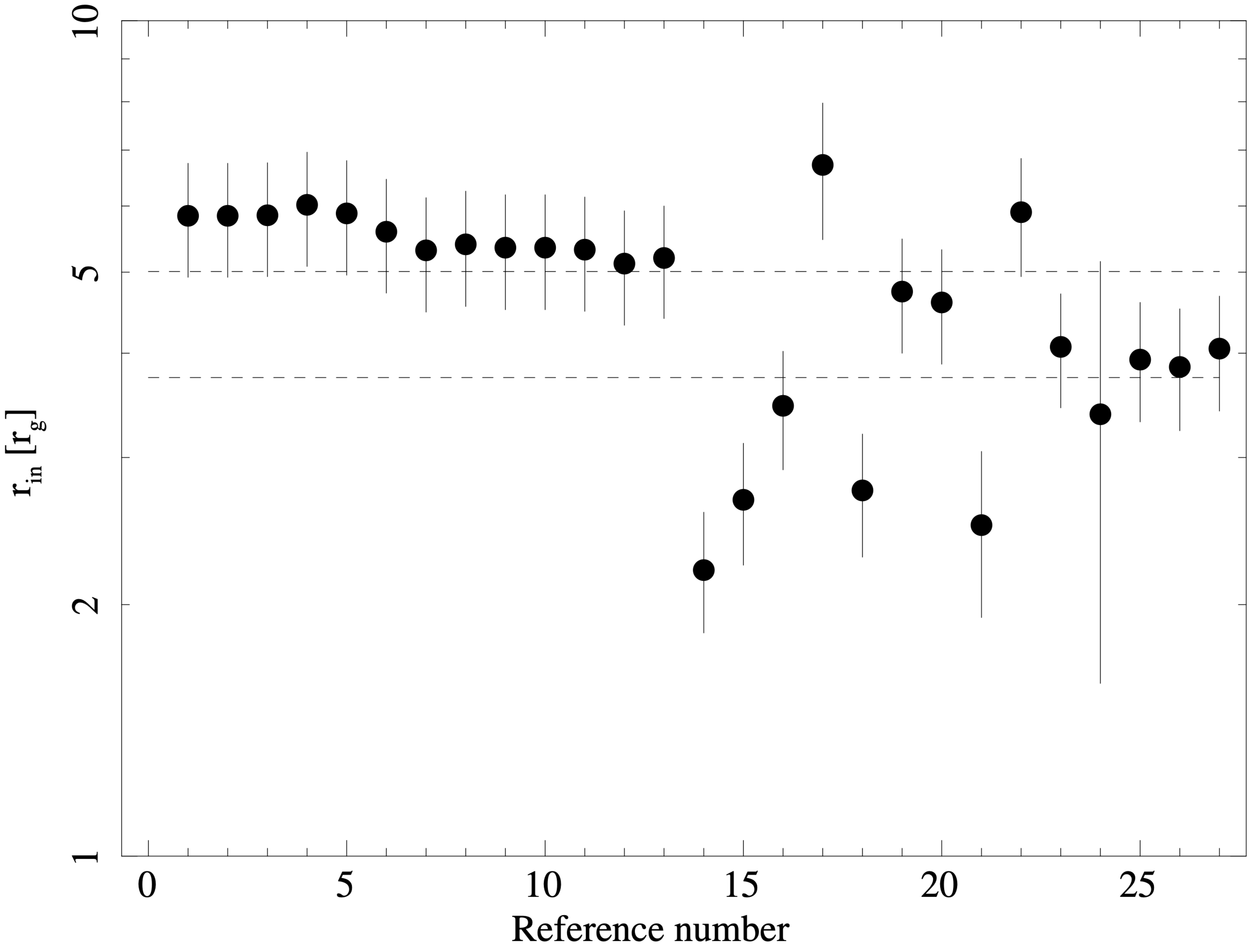

Reference numbers:
(1) Sobczak et al. (1999)
(2-13) Sobczak et al. (2000)
(14-15) Rodriguez et al. (2003)
(16) Miller et al. (2003)
(17) Kubota & Done (2004)
(18-20) Kubota & Makishima (2004)
(21) Sriram et al. (2016)
(22) Connors et al. (2019)
(23-27) Connors et al. (2020)

XTE J1550-564

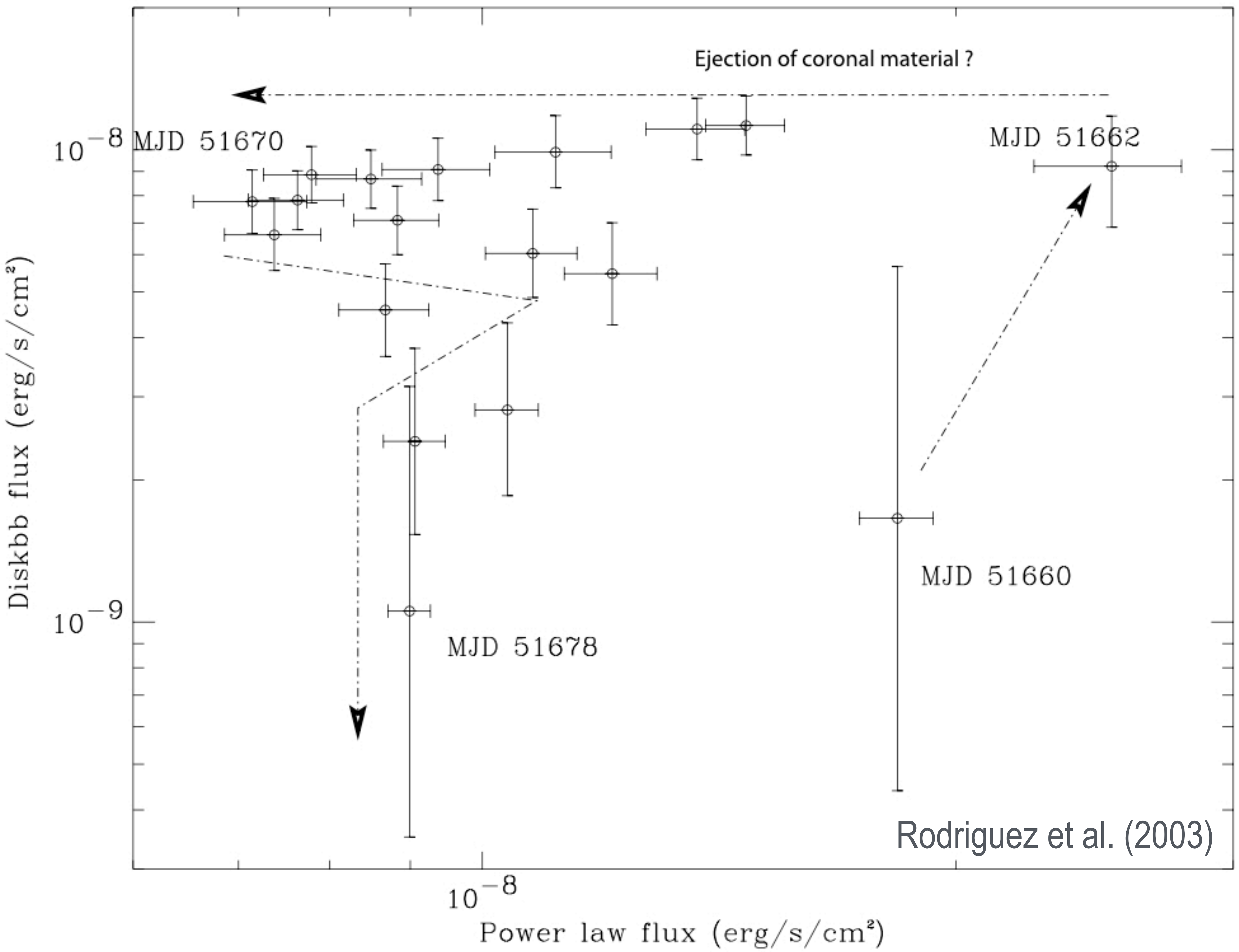

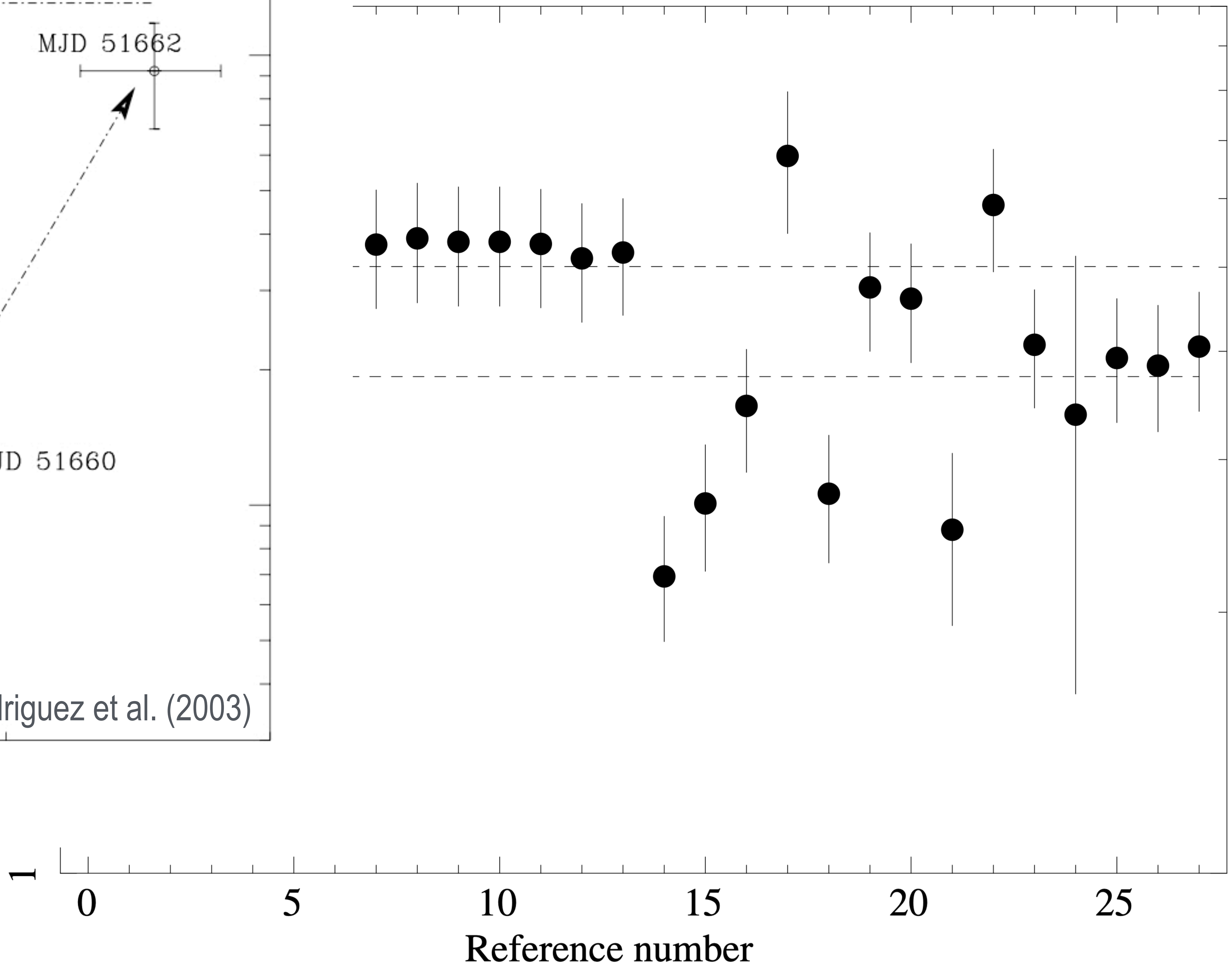

(17) Kubota & Done (2004)
(18-20) Kubota & Makishima (2004)
(21) Sriram et al. (2016)
(22) Connors et al. (2019)
(23-27) Connors et al. (2020)

XTE J1550-564

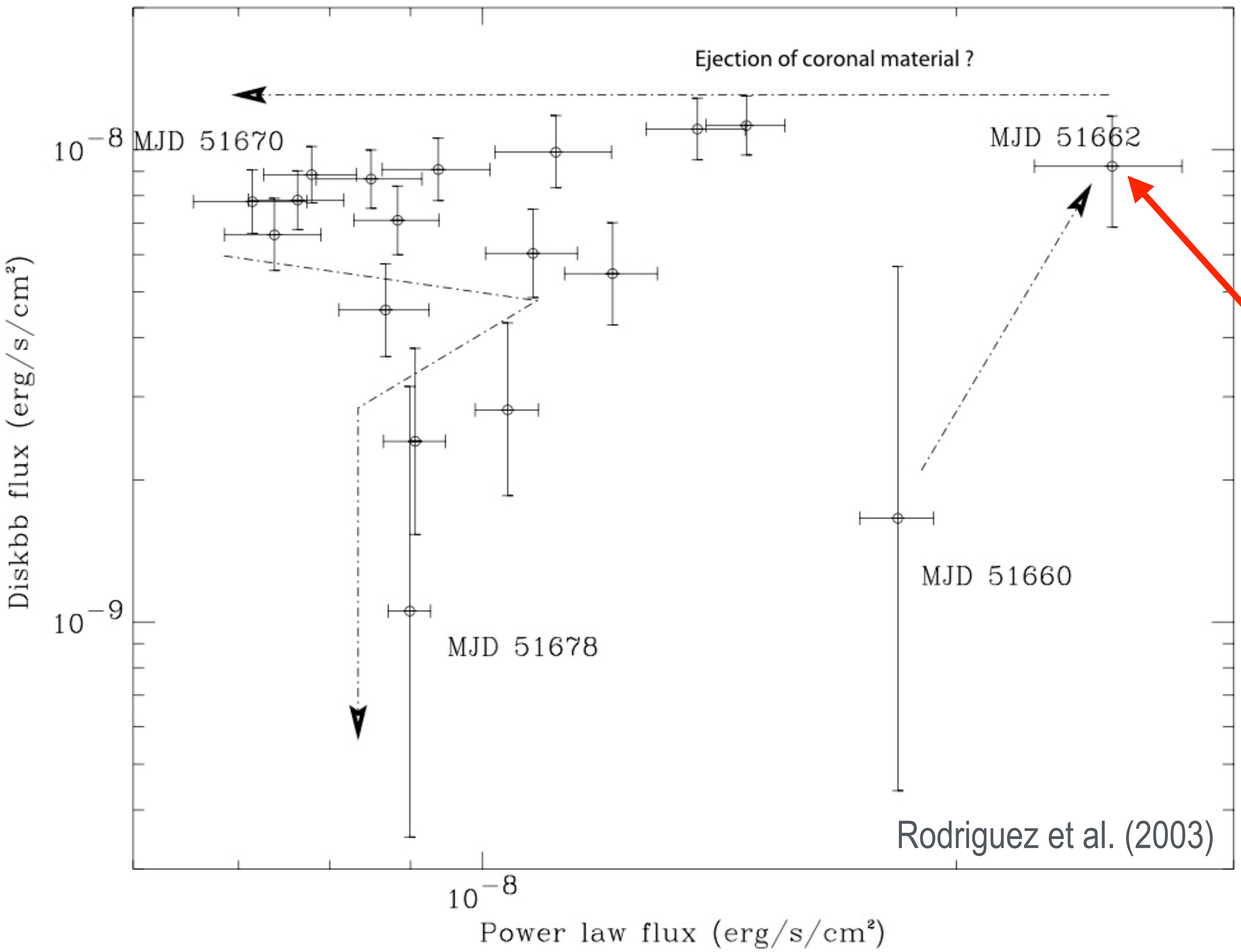

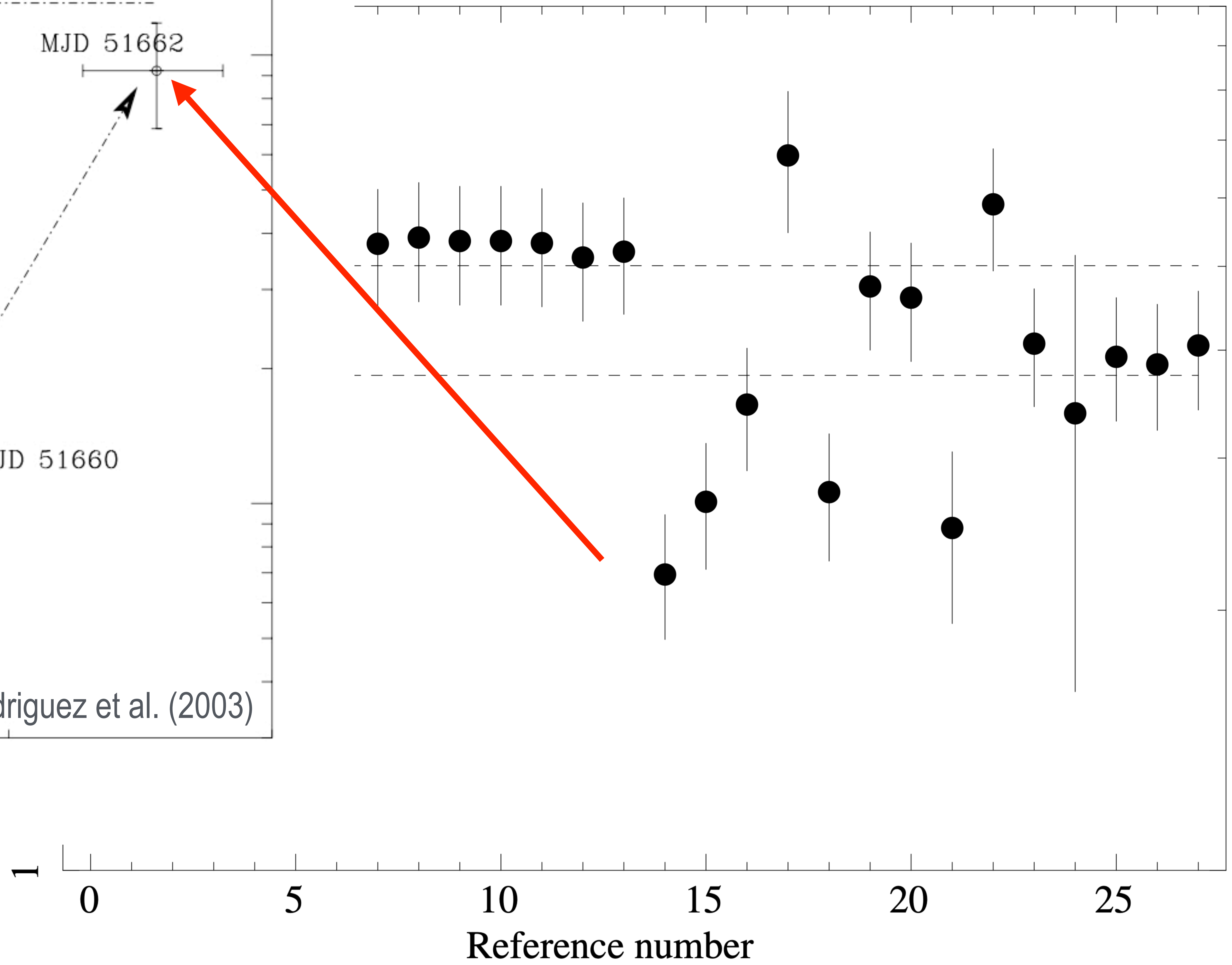

(17) Kubota & Done (2004)
(18-20) Kubota & Makishima (2004)
(21) Sriram et al. (2016)
(22) Connors et al. (2019)
(23-27) Connors et al. (2020)

XTE J1550-564

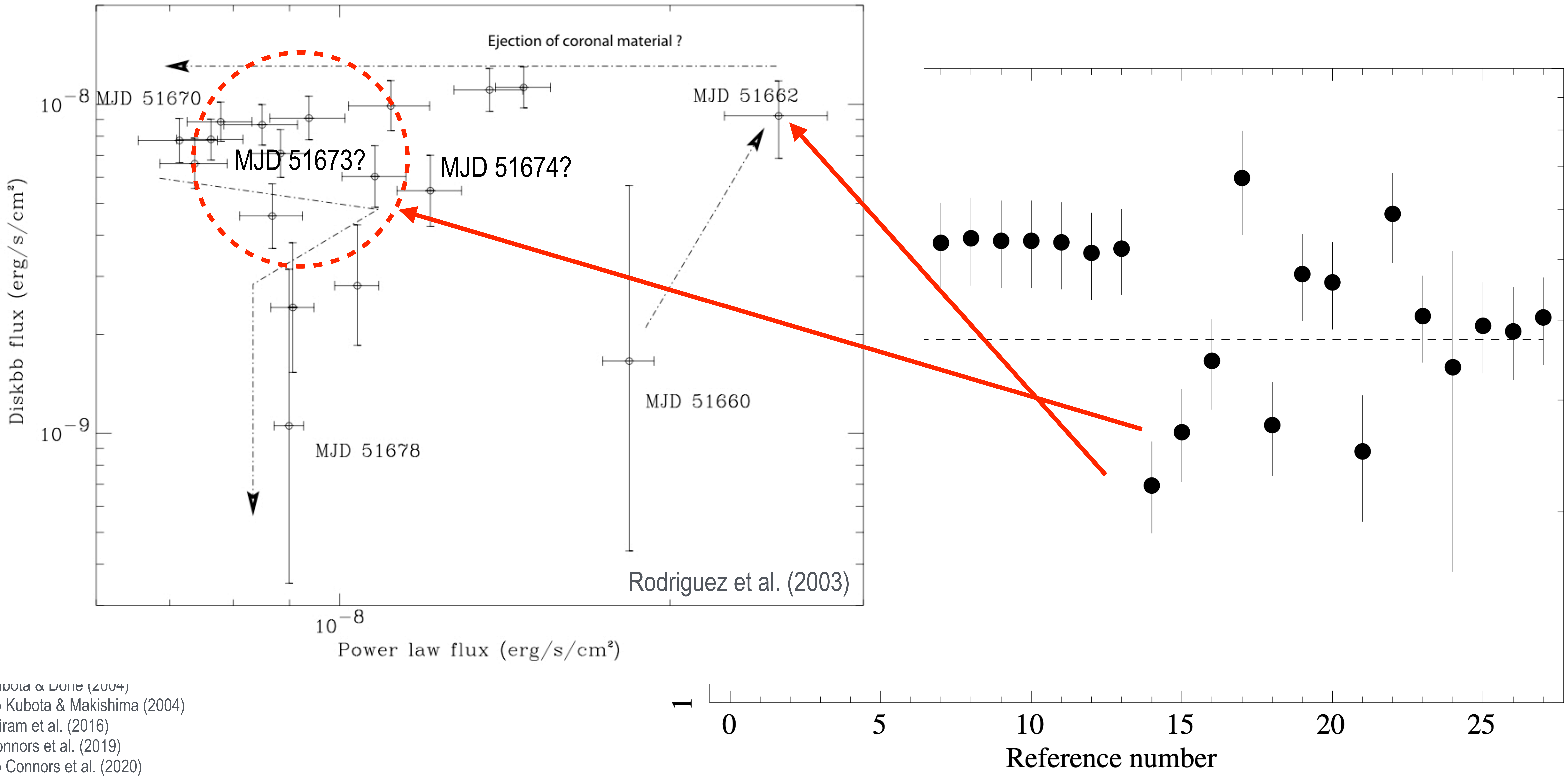

(17) Kubota & Done (2004)
(18-20) Kubota & Makishima (2004)
(21) Sriram et al. (2016)
(22) Connors et al. (2019)
(23-27) Connors et al. (2020)

XTE J1550-564

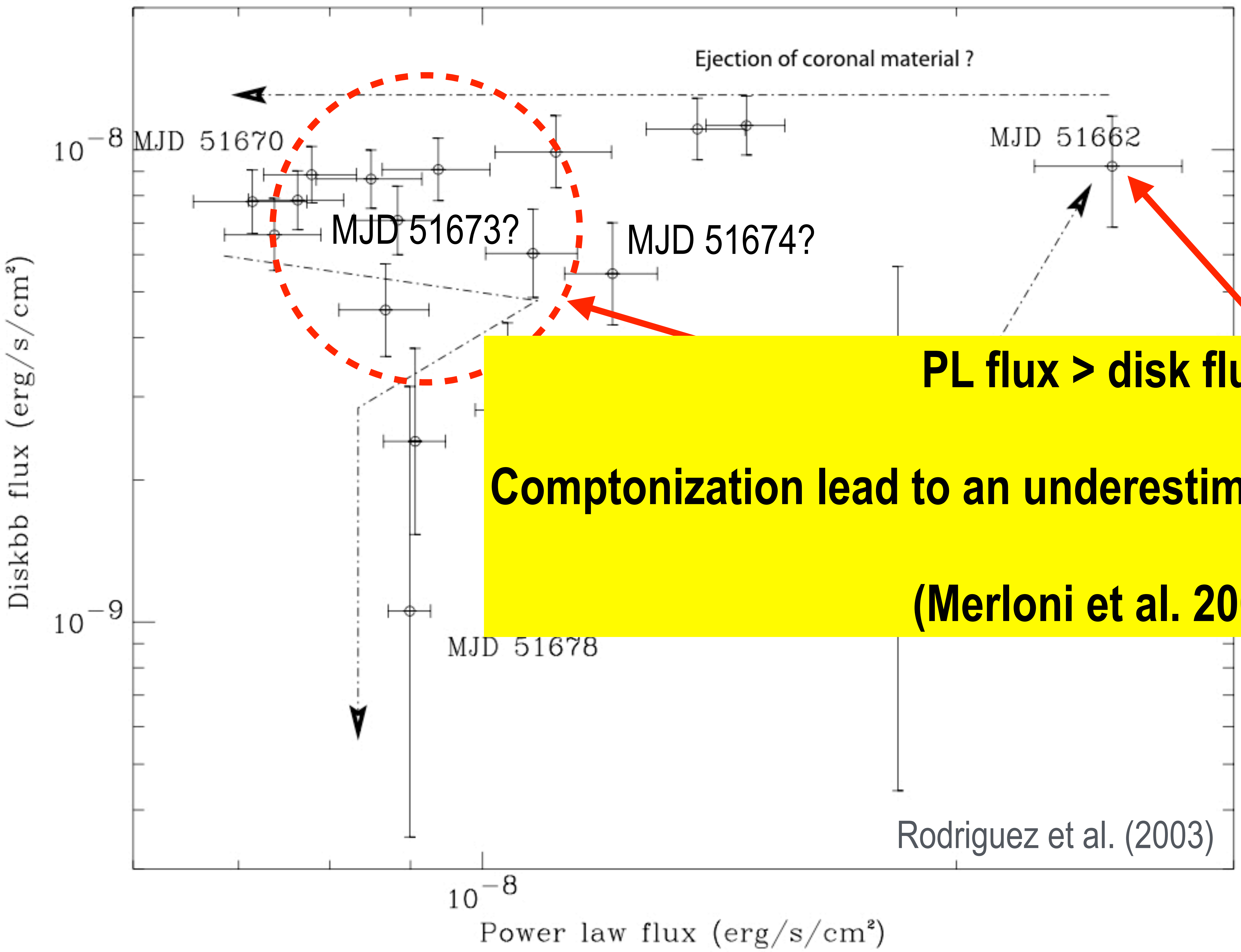

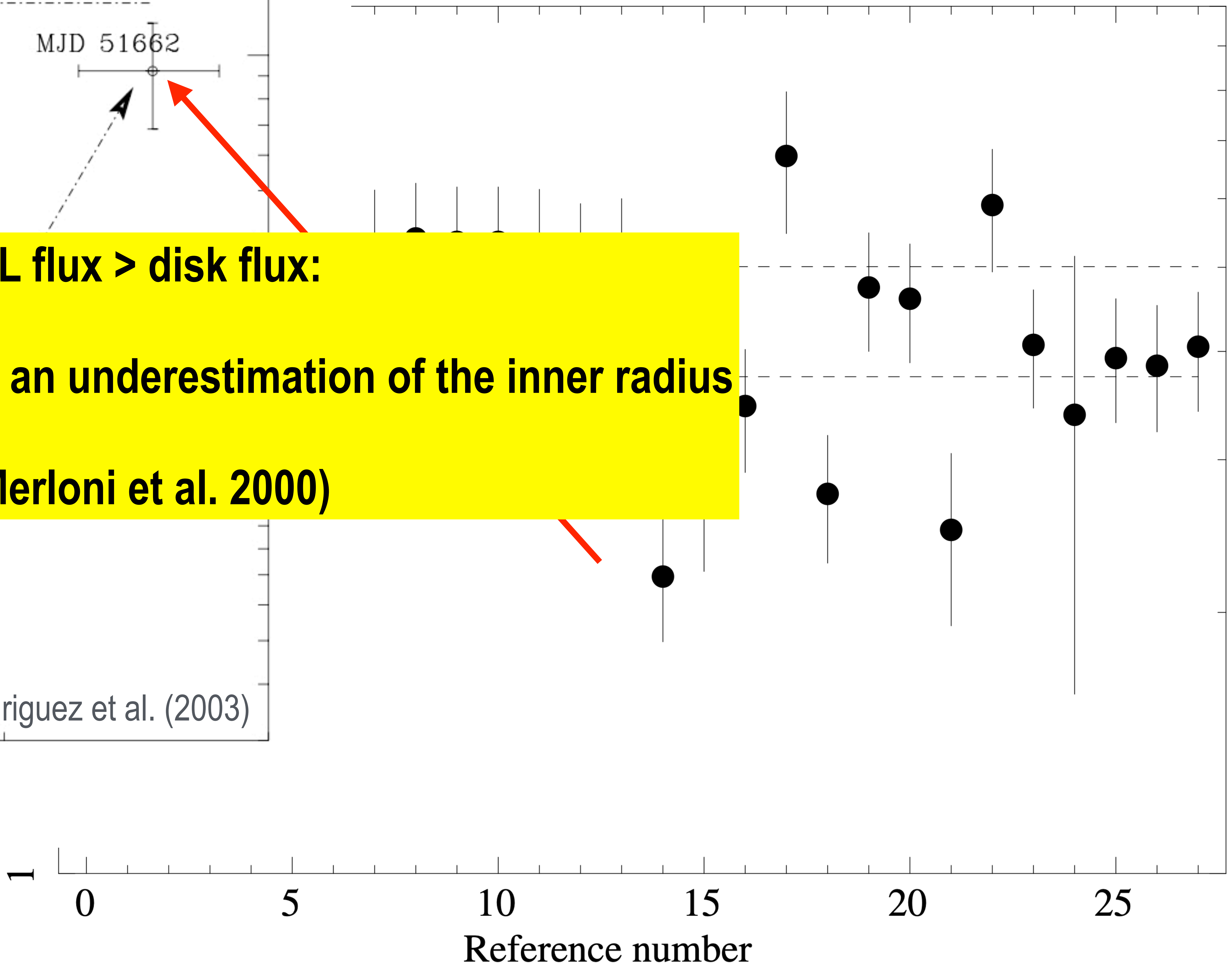

PL flux > disk flux:

Comptonization lead to an underestimation of the inner radius

(Merloni et al. 2000)

(17) Kubota & Done (2004)
(18-20) Kubota & Makishima (2004)
(21) Sriram et al. (2016)
(22) Connors et al. (2019)
(23-27) Connors et al. (2020)

GX 339-4

Reference data from Parker et al. (2016)

$$M = 9.0^{+1.6}_{-1.2}\,M_\odot \rightarrow r_g = 13 \pm 2\,\mathrm{km}$$

$$d = 8.4 \pm 0.9\,\mathrm{kpc}$$

$$i = 30^\circ \pm 1^\circ$$

$$a \sim 0.87 - 0.97$$

$$r_{\rm isco} \sim (1.73 - 2.51) r_g$$

Reference number:
(1-2) Miller et al. (2004A)
(3) Miller et al. (2004B)
(4-5) Belloni et al. (2006)
(6) Reis et al. (2008)
(7) Miller et al. (2008)
(8-10) Del Santo et al. (2008)
(11-13) Motta et al. (2009)
(14-18) Caballero-Garcia et al. (2009)
(19) Shidatsu et al. (2011)
(20) Motta et al. (2011)
(21) Tamura et al. (2012)
(22) Rahoui et al. (2012)
(23) Plant et al. (2014)
(24-25) Ludlam et al. (2015)
(26) Kubota & Done. (2016)
(27-29) Stiele & Kong (2017)
(30-33) Sridhar et al. (2020)
(34-36) Shui et al. (2021)
(37) Liu et al. (2022)
(38-40) Yang et al. (2023)
(41) Peirano et al. (2023)
(42) Liu et al. (2023)
(43) Jana et al. (2024)

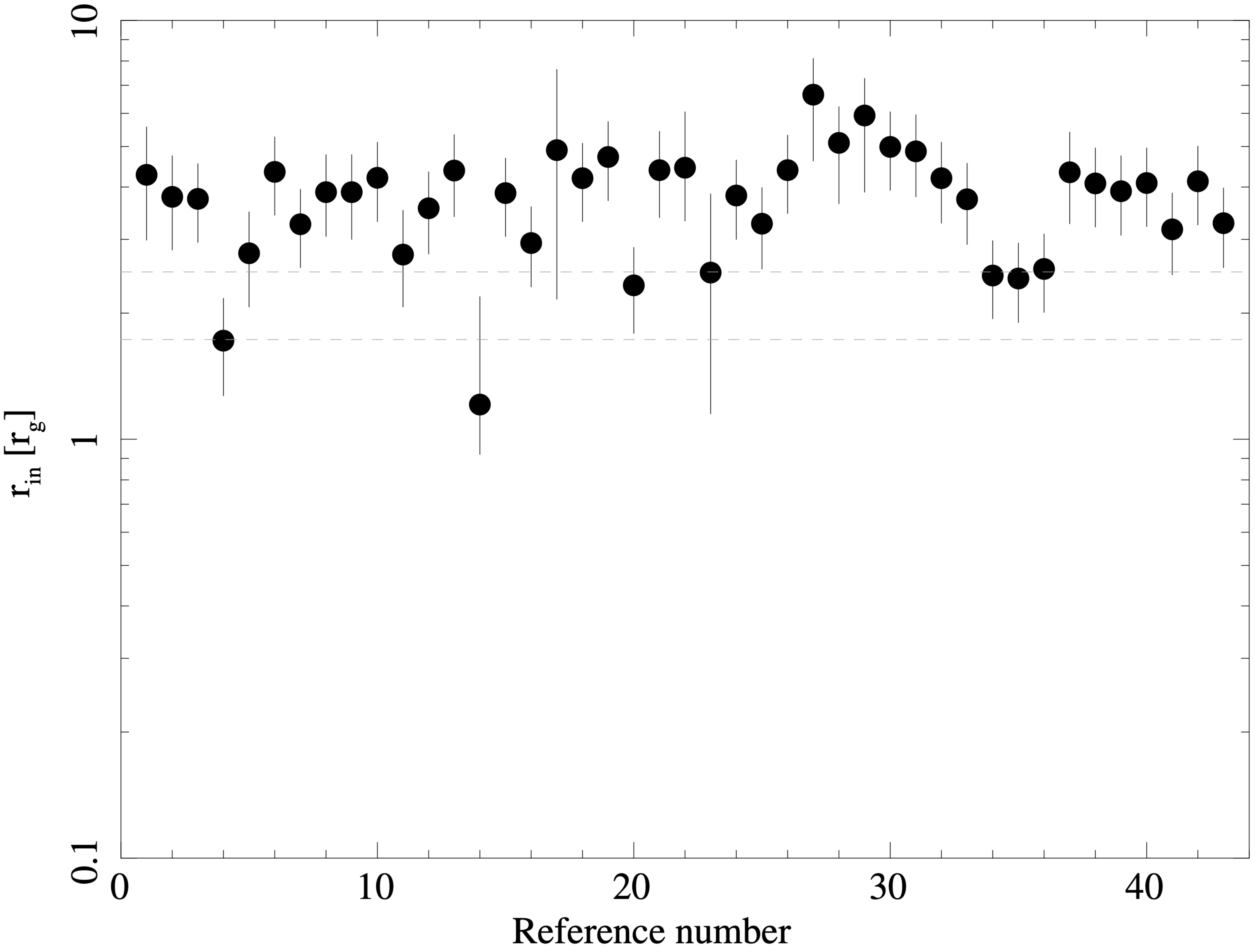

XTE J1650-500

Reference data from Orosz et al. (2004), Homan et al. (2006), Slany & Stuchlik (2008)

$$M = 4.0 \pm 0.6\, M_\odot \rightarrow r_g = 5.9 \pm 0.9\,\mathrm{km}$$

$$d = 2.6 \pm 0.7\,\mathrm{kpc}$$

$$i = 70^\circ \pm 4^\circ$$

$$a \sim 0.9982$$

$$r_{isco} \sim 1.23 r_g$$

Only two cases found:

- Miller et al. (2002): $r_{in} = 18 \pm 8 r_g$
- Miniutti et al. (2004): $r_{in} = 5.3 \pm 1.7 r_g$

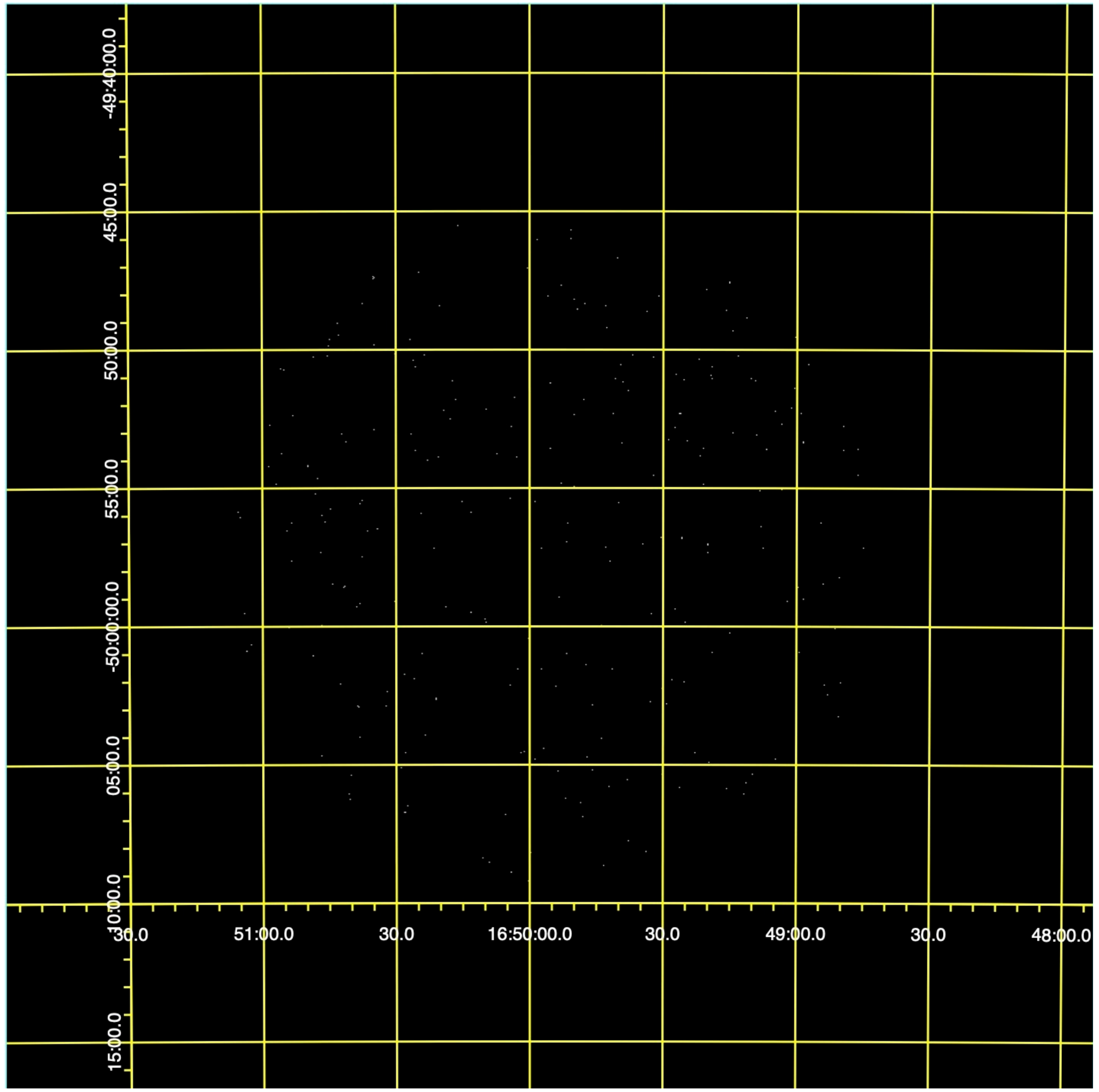

One *Swift* archival observation with exposure ~ 1 ks: no source detected.

GRO J0422+32: the smallest black hole?

Reference data from Casares et al. (2022), Gelino et al. (2003)

$$M = 2.7^{+0.7}_{-0.5}\,M_\odot \rightarrow r_{\rm g} = 4.0^{+1.0}_{-0.7}\,\mathrm{km}$$

$$d = 2.49 \pm 0.30\,\mathrm{kpc}$$

$$i = 55^\circ 6 \pm 4^\circ.1$$

$$a \sim ?$$

$$r_{\rm isco} \sim ?$$

Only one cases found:

- Shrader et al. (1997): $r_{\rm in} = 5.1 \pm 2.3 r_{\rm g}$

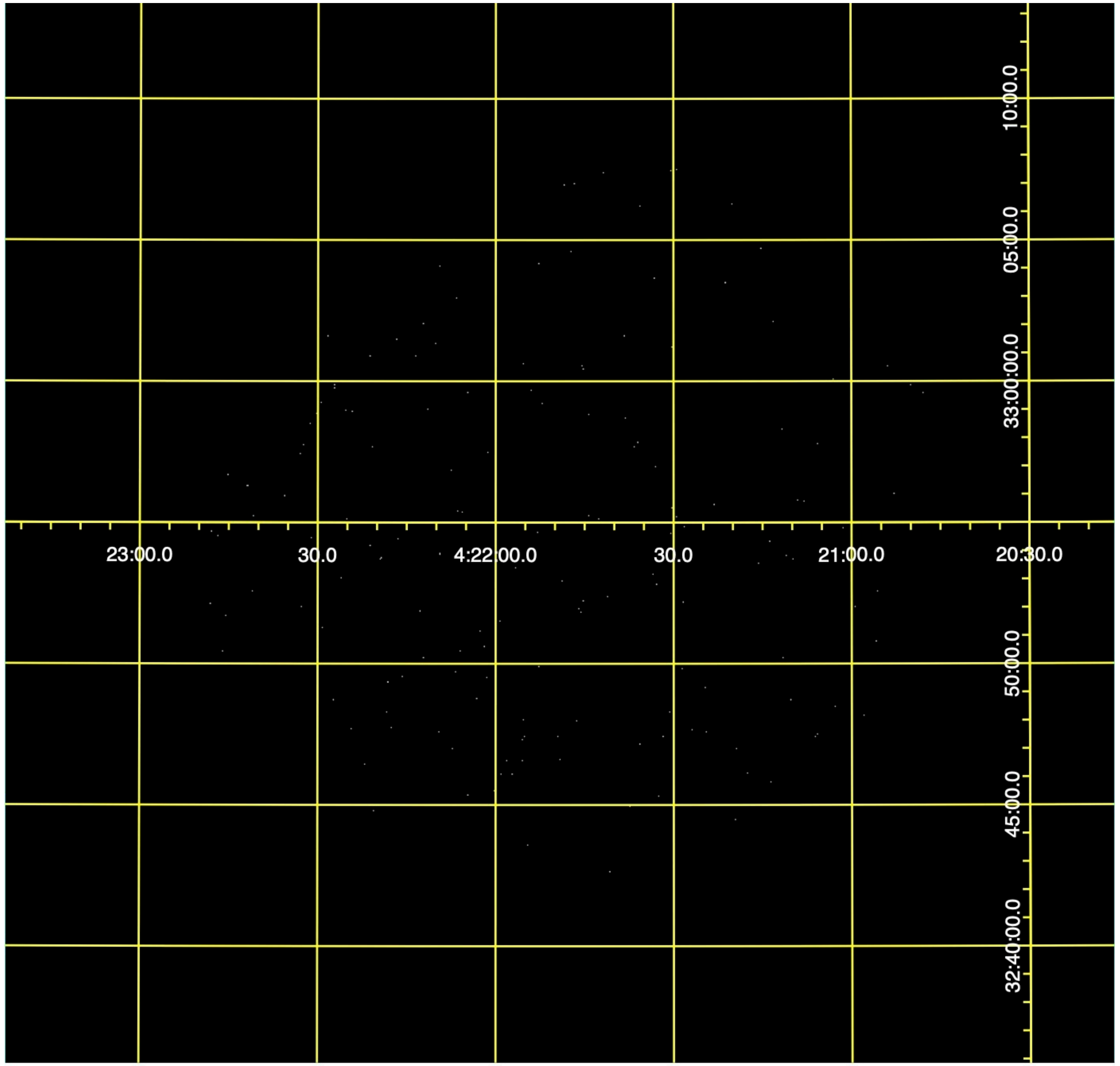

One *Swift* archival observation with exposure ~ 1.2 ks: no source detected.

Final remarks

- **All the measured radii are consistent with the expectations of general relativity;**

- A few anomalous cases can easily be reconciled by taking into account the impact of Comptonization, a proper selection of the hardening factor, the doubts on the reference quantities, and the instrumental biases;

- What can we say about ξ?
  - **This method is not suitable for negative values of** ξ, because it implies an increase of $r_{\rm isco}$. However, $r_{\rm isco}$ can change when the object is in different states, because of known physical processes. The extreme case of truncated inner disk occurs in hard state ($r_{\rm isco}$ at tens of $r_{\rm g}$), with the blown up of the corona and the onset of the jet.
  - By considering the **best case (Cygnus X-1, Tomsick et al. 2014)**, we can set a constraint on the positive values of ξ:

$\tilde{\xi} = \dfrac{\xi}{r_{\rm g}^2} \gtrsim 0.028\,(3\sigma)$ by assuming $a \sim 0.98$ (arithmetic mean of the measured values).

- Work to do:
  - improve the measurements of the reference quantities: the spin is the most critical one;
  - It is important to address the impact of Comptonization via either the hardening factor or a more detailed spectral modelling;
  - improve instrumental biases: modern detectors have lower energy thresholds, but are much more sensitive (difficult to cope with very high fluxes, pile-up problems);